Potential knowledge gain in large-scale simulations of forest carbon fluxes from remotely sensed biomass and height

Valentin Bellassen, Nicolas Delbart, G. Le Maire, S. Luyssaert, Philippe Ciais, N. Viovy

Title: Potential knowledge gain in large-scale simulations of forest carbon fluxes from remotely sensed biomass and height

Journal: Forest Ecology and Management, Elsevier, 2011, 261 (3), pp.515. ⟨10.1016/j.foreco.2010.11.002⟩.

Authors: Bellassen V[1], Delbart N[1], Le Maire G[2], Luyssaert S[1], Ciais P[1], Viovy N[1]

[1]Laboratoire des Sciences du Climat et de l'Environnement, Commissariat à l'énergie atomique / CEA-Orme des Merisiers / F-91191 Gif-sur-Yvette CEDEX / France

[2]CIRAD, Persyst, UPR 80, s/c UMR Eco&Sols, 2 Place Viala - bât 12, 34060 Montpellier cedex 01, France

Corresponding author: Bellassen V

Phone: +33 1 69 08 31 01

Fax: +33 1 69 08 30 73

E-mail: valentin.bellassen@lsce.ipsl.fr

Abstract

Global Vegetation Models (GVMs) simulate CO_2, water and energy fluxes at large scales, typically no smaller than 10 x 10 km. GVM simulations are thus expected to simulate the *average* functioning, but not the *local* variability. The two main limiting factors in refining this scale are 1) the scale at which the pedo-climatic inputs – temperature, precipitation, soil water reserve, etc. – are available to drive models and 2) the lack of geospatial information on the vegetation type and the age of forest stands. This study assesses how remotely sensed biomass or stand height could help the new generation of GVMs, which explicitly represent forest age structure and management, to better simulate this local variability. For the ORCHIDEE-FM model, we find that a simple assimilation of biomass or height brings down the root mean square error (RMSE) of some simulated carbon fluxes by 30-50%. Current error levels of remote sensing estimates do not impact this improvement for large gross fluxes (e.g. terrestrial ecosystem respiration), but they reduce the improvement of simulated net ecosystem productivity, adding 13.5-21% of RMSE to assimilations using the *in situ* estimates. The data assimilation under study is more effective to improve the simulation of respiration than the simulation of photosynthesis. The assimilation of height or biomass in ORCHIDEE-FM enables the correct retrieval of variables that are more difficult to measure over large areas, such as stand age. A combined assimilation of biomass and net ecosystem productivity could possibly enable the new generation of GVMs to retrieve other variables that are seldom measured, such as soil carbon content.

Keywords: remote sensing; global vegetation model; ORCHIDEE; carbon; biomass; height

1 Introduction

Along with the growing concern about climate change, international agreements and regional markets have appeared and now give an economical value to carbon. These developments have naturally led to look at forest services from a carbon perspective: what is the carbon budget of a country's forests and how will it evolve? How can forest management increase the carbon balance of a forest stand and how can this mitigation effort be rewarded? To answer these questions, policy makers and foresters have progressively turned to forest models.

Stand-scale growth-and-yield models – such as FAGACEES (Dhôte and Hervé, 2000), SILVA (Pretzsch *et al.*, 2002) or CO2FIX (Masera *et al.*, 2003) – or process-based models – such as CASTANEA (Dufrene *et al.*, 2005) or GRAECO (Porté, 1999) – offer trustworthy local simulations of carbon stocks. Nevertheless, the former require a local site productivity index and the latter tend to require an intensive local calibration, based on extensive field observations. It renders both types of models very site-specific and unfit to simulate regional fluxes and stocks. Another solution is to use generic global vegetation models such as Ecosytem Demography (Moorcroft *et al.*, 2001), Biome-BGC (Thornton *et al.*, 2002), LPJ (Sitch *et al.*, 2003) or ORCHIDEE (Krinner *et al.*, 2005). Although these GVMs tend to perform worse than well calibrated stand-scale models on a site-by-site basis (Loustau *et al.*, 2005), they provide estimates of carbon stocks and fluxes at regional scales, or where data is lacking for a local calibration. Their estimates of continental carbon budgets are within the range given by other methods (Lindner *et al.*, 2004), but uncertainty remains high: for the carbon balance of European forests (EU25), the estimates of three similar GVMs exhibit a 2-fold difference (Luyssaert *et al.*, 2010).

The bigger uncertainty of GVM estimates has two main causes: first the pedo-climatic inputs driving the models are too coarse and do not capture local variations, which in turn can generate errors due to the non-linear response of physiological processes to these inputs. Second most GVMs do not explicitly simulate management (Le Quere *et al.*, 2009), and therefore fail to correctly simulate age-dependent variables such as aboveground biomass. This pitfall is being increasingly addressed (Zaehle *et al.*, 2006; Desai *et al.*, 2007; Sato *et al.*, 2007; Bellassen *et al.*, 2010a).

In even-aged stands, local variations of soil fertility, climate, and stand age can be combined in the notion of "growth stage". Forest yield tables indeed show that most characteristics – stand density, height, basal area, diameter, aboveground biomass, ... – of two stands with different fertility classes follow the same evolution with age, albeit not at the same pace (Vannière, 1984; JRC, 2009). A 50 year old forest standing on a productive site may be considered to be at the same "growth stage" than a 100 year old forest standing on an unfertile soil, as they have similar biomass and height. Information about the "growth stage" of forest stands could be used to account for sub-grid heterogeneity in GVM simulations and increase the match between simulations and local measurements. Initializing a GVM with a spatially explicit map of growth stage may improve simulations in two ways: 1) at the local level, information on growth stage recreates some intra-pixel variability in simulations which may improve the fit to site data and 2) at the continental level, a map of growth stage provides a spatially more precise initialization than the current regional or national age averages of forest inventories. The

initialization of carbon pools has already been shown to play an important role in the ability of GVMs to reproduce local flux data (Carvalhais *et al.*, 2010).

Both average stand height and aboveground biomass could be estimated at large scales with active remote sensing techniques such as RADAR and LiDAR. These two variables can therefore be used to initialize growth stage in a model simulation. P-band RADAR has been particularly used for estimating biomass, as the reflected signal is more specific to the woody components of trees, and therefore saturates at higher levels of biomass than other techniques (Le Toan *et al.*, 2008). The LiDAR signal is less specific and most often used to estimate canopy height structure. Many studies however derive biomass estimates from LiDAR measurements, using the allometric relationship between biomass and height (Lim and Treitz, 2004; Lefsky *et al.*, 2005b; Stephens *et al.*, 2007; Naesset, 2009). Except for a few data from the GLAS LiDAR satellite (Lefsky *et al.*, 2005a; Boudreau *et al.*, 2008), all P-band RADAR and LiDAR studies relied on airborne campaigns, and were therefore limited to the local scale. As the European Space Agency is currently assessing the need for a P-band RADAR satellite (Le Toan *et al.*, 2008) and a LiDAR satellite (Durrieu, 2010), there is a pressing need to quantify the benefits of remotely sensed biomass or height for the new generation GVMs which simulate different stand growth stages.

To this aim the current study compares the standard version of the ORCHIDEE GVM, with steady-state equilibrium forests, to a more recent version, ORCHIDEE-FM, that simulates forest management and the resulting tree height and biomass in a generic – that is even-aged – managed stand. The ability of ORCHIDEE-FM to simulate the growth stages of a forest stand is

checked with forest inventory plots. Then, pseudo-RADAR and LiDAR estimates of height and biomass are generated, based on existing *in situ* measurements from forest inventories and a global flux database. These pseudo-measurements are used to initialize ORCHIDEE-FM, and the improvement brought by this basic data assimilation is quantified for the simulation of volume increment, gross primary production (GPP), total ecosystem respiration (TER) and net ecosystem productivity (NEP). These quantified improvements provide a first assessment of the knowledge that could be gained from remotely sensed "growth stage" maps for large-scale carbon and water flux estimates.

2 Material and Methods

2.1 Field data

Two in situ datasets are used in this study: the French national forest inventory (IFN) plots in two different regions, and the global flux and biometry database of Luyssaert *et al.* (2007).

2.1.1 French national forest inventory (IFN)

The first in situ dataset used in this study comes from the French national forest inventory (IFN). The IFN conducts yearly field measurement campaigns covering the entire French metropolitan territory. A systematic inventory grid is visited and inventoried following the IFN protocol (IFN, 2006): circumference at breast height, width of the last five rings, height and species are recorded for a representative sample of trees. IFN allometric rules are used to estimate commercial volume and volume increment. For even-aged stands, a few tree cores

sampling all growth rings are used to estimate stand age class, with age class widths between 10 and 20 years. Raw data for each plot is available on the IFN website (www.ifn.fr).

When necessary, estimated standing volume is converted to total aboveground biomass, using the default branch ratio and carbon density parameters of ORCHIDEE-FM (Table 1). Furthermore, commercial wood increment is used to estimate annual woody Net Primary Productivity (NPP), using Eq. 1.

$$NPP_{woody} = (I + \varepsilon) \times (1 + T_b \times br \times V) \times BEF_i \times d_w \times d_c \quad (1)$$

where NPP_{woody} is the annual woody NPP in gC m^{-2} yr^{-1}, I is the estimated commercial wood increment in m^3 m^{-2} yr^{-1}, T_b is the annual turnover of branches in yr^{-1}, br is the total branch ratio (no unit), V is the estimated standing commercial wood in m^3 m^{-2}, ε is the averaged increment of trees that died over the last five years before measurement in m^3 m^{-2} yr^{-1}, BEF_i is the biomass expansion factor for volume increment (no unit), d_w is the wood density in gDM m^{-3} (grams of dry matter), and d_c is the carbon density in gC gDM^{-1}. At most a few percent of trees commonly die over 5 years. They are usually smaller trees and not all die right before measurement date. ε is therefore much smaller than the wood increment of trees which survived, and neglected in the calculations. For parameter values, see Table 1.

For this study, the results of three campaigns – 2005, 2006 and 2007 – are pooled, and only even-aged stands are used. To assess the performance of ORCHIDEE-FM, we selected regions that filled the following criteria:

- As REMO climate input data have a 0.25° x 0.25° resolution (see section 2.3.2) we selected grid points where climate does not vary strongly at the considered spatial scale

so that a single ORCHIDEE-FM simulation should be representative of neighbouring IFN plots

- A second criteria is to have enough IFN plots within a 0.5° radius for statistical purposes.

Two highly forested regions fit these criteria for both broadleaves and needleleaves: southwestern and northeastern France. We therefore selected one southwestern gridpoint, hereafter referred to as "Landes", and one northeastern gridpoint, hereafter referred to as "Vosges", with respectively 215 and 324 IFN plots within a 0.5° radius of the grid point centre. The characteristics of these two grid points are summarized in Table 2. The IFN dataset thus provides a high number of *in situ* estimates for age, average height, standing aboveground biomass, and woody NPP at various growth stages (stand ages vary from 2 to 200 years). However, it does not provide direct carbon fluxes measurements.

2.1.2 Global dataset for carbon fluxes

Luyssaert *et al.* (2007) compiled a dataset of carbon flux measurements on forest sites, heavily building on the eddy covariance FLUXNET network (Baldocchi *et al.*, 2001). This dataset also gives additional site information, when available, regarding stand age, average height and biomass. All managed sites in temperate and boreal biomes informed for stand age, average height and aboveground biomass, and either GPP, TER or NEP were retained for this study, thus reducing the database to a subsample of 31 sites. When several years of measurements were available for a given variable, the average was retained. The resulting dataset, hereafter referred to as the "global flux dataset", is presented in Appendix A.

Three peculiar site configurations are beyond the expected validity domain of ORCHIDEE-FM and therefore excluded for the quantification of performance improvement:

- Forest stands younger than 20 years (8 sites): in such young stands, NEP is expected to be heavily influenced by the site history before stand establishment (eg. afforested farmland or clearcut old stand) for which we have no information. This hypothesis is tested by analyzing the difference in simulations with two extreme sets of initial conditions: forest regrowth – initial conditions corresponding to the clear-cut of a mature forest – and reforestation – initial conditions corresponding to a cropland.
- Carbon sources (2 sites): our dataset only contains growing managed stands younger than 103 years old. Such stands are not expected to be net sources of carbon for several years in a row, unless management events such as heavy thinnings or clear-cuts take place within the footprint of the flux tower. Again, the absence of information on such heavy management events makes it hazardous to simulate these sites.
- Collelongo (1 site): GPP at this 103 years old Italian site is twice larger than TER, which makes it an outlier in most analysis of the global flux database (Luyssaert *et al.*, 2009). In our case, climate is a possible explanation as it exhibit strong local variations – uncaptured by the 0.25° resolution forcing data – in this part of Italy.

The resulting dataset of 20 sites is hereafter referred to as the “screened dataset”.

2.2 Generation of pseudo remote sensing data

The *in situ* estimates of average stand height and biomass from the two datasets are used to construct a set of pseudo remote sensing estimates of these variables. To this end, a random

error is added to the *in situ* estimates of height and biomass. This random error is drawn from a normal probability law centred on the *in situ* estimate and with a standard deviation equal to the typical RMSE of LiDAR and P-band RADAR estimates of average height and biomass. This implies three assumptions: *in situ* estimates are assumed to be perfect, remote sensing observations are assumed to be unbiased and their error is assumed to be independent of the estimate value. The typical RMSE assigned to these pseudo-remote sensing observations are averages of RMSE from relevant literature studies (see Table 3): the typical RMSE of LiDAR is lower than that of RADAR for average height (1.66 vs 2.34 m) and higher for average biomass (23.7 vs 18.5 tC ha^{-1}). The procedure of "pseudo data" generation is repeated 10 000 times – procedure based on the Monte Carlo technique (Rubinstein and Kroese, 1981) – for each *in situ* estimate in order to generate a representative pseudo-dataset.

2.3 Model

2.3.1 ORCHIDEE and ORCHIDEE-FM

The ORCHIDEE global vegetation model ("ORganizing Carbon and Hydrology In Dynamic Ecosystems") is designed to operate from regional to global scales (Krinner *et al.*, 2005). ORCHIDEE typically represents an average mature forest at steady-state equilibrium in a "big-leaf" approach. For a given climatology, it simulates the carbon, water and energy budget at the pixel scale. For carbon, ORCHIDEE computes its assimilation (GPP), allocates photosynthates to the different biomass compartments where they are respired or stored, and recycles carbon through constant tree mortality and soil respiration. This "standard" version of ORCHIDEE

(V1.9.4) is intended to simulate forests that have reached a steady-state equilibrium between growth and mortality. Its uses the allocation framework of Friedlingstein *et al.* (1999), and does not simulate the nitrogen cycle, recently included in ORCHIDEE-N by Zaehle and Friend (2010). This version of ORCHIDEE, hereafter referred to as the standard version, is intended to simulate forests that have reached a steady-state equilibrium between growth and mortality.

The standard version does not represent important processes driving the evolution of stand structure such as competition, forest management, or the age-limitation of NPP and is therefore not suited to simulate managed forests, or forests recovering from past disturbance. As a consequence of its formulation all carbon pools, including biomass, need to be put to equilibrium before studying the effect of varying climate and CO_2 conditions. This equilibrium is obtained by a "spin-up", that is an initial simulation which stops when carbon and water pools are in equilibrium with a fixed climate which can take up to 10 000 years.

In order to simulate forest management, several processes have been added to the standard version of ORCHIDEE, among which a Forest Management Module (FMM) inspired from the stand-level model FAGACEES (Dhôte and Hervé, 2000). The key concept is to add to the "average tree" representation of ORCHIDEE an explicit distribution of individual trees, which is the basis for a process-based simulation of mortality. The aboveground "stand-scale" wood increment simulated by ORCHIDEE is distributed among individual trees according to the rule of Deleuze et al. (2004): the basal area of each individual trees grows proportionally to its circumference. Tree mortality is then determined by the structure of the stand. Mortality due to natural competition relies on the self-thinning rule of Reineke (1933) while another set of

rules drives the mortality processes due to human interventions such as thinnings or clearcuts. Some other small refinements have been added to ORCHIDEE such as a height limitation on leaf area index (LAI) and an age-related decline in photosynthesis efficiency. As a result, this new version of the model, called ORCHIDEE-FM, is able to simulate the carbon budget and detailed stand structure of forests of varying ages (Bellassen *et al.*, 2010b). Its equations are fully described in Bellassen et al. (2010a). For both versions of the model, the standard value of the maximum rate of carboxylation, Vc_{max}, is set to the optimized values for 6 sites in France and Germany found by Santaren (2006) for needleleaves and broadleaves, that is respectively 42.6 and 52.2 in µmol m^{-2} s^{-1}.

2.3.2 Simulations

2.3.2.1 Input data

For simulations at the sites of the global flux dataset, the climate forcing data comes from the 2.5° resolution NCEP – National Centers for Environmental Prediction – reanalysis, adjusted with the 0.5° CRU – Climate Research Unit – data for temperature and precipitation and interpolated to a 0.5° resolution (Kalnay *et al.*, 1996; Mitchell and Jones, 2005). As in most global simulations (Krinner *et al.*, 2005), the soil bucket is uniformly taken to be 2 m deep and its texture is evenly distributed between clay, sand and silt, corresponding to a uniform water holding capacity of 300 mm

For the IFN sites, we use the 0.25° resolution REMO reanalysis (Vetter *et al.*, 2008), which covers Europe. Maps of soil depth and texture were derived from FAO and IGBP products (Vetter *et al.*, 2008).

2.3.2.2 Model "spinup"

Following a standard method in GVM modelling, a model "equilibrium spinup" is performed before all simulations to define the initial conditions of subsequent simulations, in particular for soil carbon. For this "spinup", ORCHIDEE is repeatedly run for the climate of the 10 years preceding stand establishment until all ecosystem carbon and water pools, including soil, reach a steady-state equilibrium. For the ORCHIDEE-FM simulations, the runs start with a clear-cut: stems are exported and all the remaining biomass – branches, roots and leaves – goes to the litter pools, except for a small fraction corresponding to the initial stand structure assumed by the model.

2.3.2.3 Simulation set up

The reference simulation – *STD* – uses the standard version of ORCHIDEE. This simulation is compared to seven simulations using ORCHIDEE-FM, the age-explicit version of the model. For each grid point, ORCHIDEE-FM is run 15 times, with plantation dates spanning 150 years before the date of observation, in order to capture all the growth stages potentially existing on the grid point. Out of these 15 runs, seven simulations are then selected for comparison with the reference simulations: FM_{ga}, FM_{gb} and FM_{gh}, the simulations with respectively the closest age, biomass and height to the actual *in situ* estimate. FM_{lb} and FM_{lh} are the simulations with the respectively closest biomass and height to the pseudo-lidar measurement. FM_{rb} and FM_{rh} are

263 the simulations with respectively closest biomass and height to pseudo-radar measurement.
264 This selection is in fact a basic synthetic data assimilation procedure (Piao *et al.*, 2009) assuming
265 a perfect model and random errors only: the starting date of ORCHIDEE-FM simulations is
266 chosen among different realizations in order to minimize the absolute difference between a
267 simulated variable – age, biomass, or height – and its measured counterpart. The simulation
268 procedure is summarized in

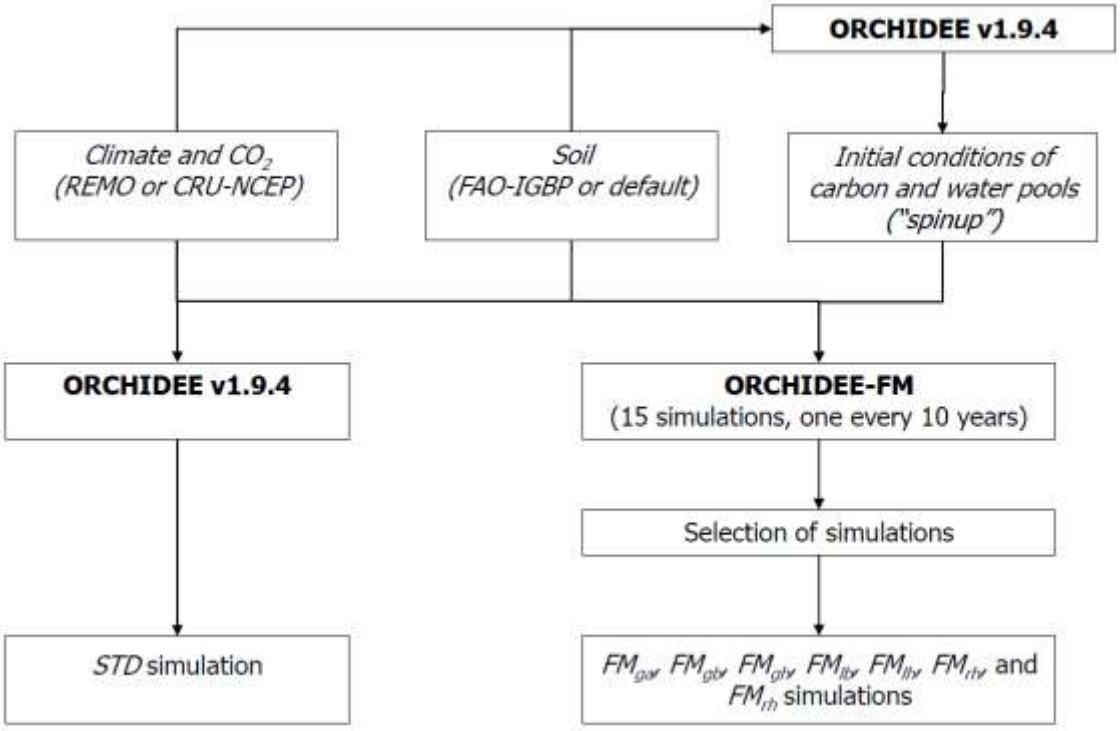

269

270 Figure 1 and simulations names are summarized in Appendix E, together with other
271 abbreviations.

2.4 Model assessment and quantification of simulation improvement

2.4.1 Assessment of stand growth simulation

The expected improvement of ORCHIDEE-FM simulations relies on the assumed ability of the model to correctly simulate the evolution of forest stand variables such as height and biomass as a function of age. To check this ability, two tests are performed: first, the simulated evolution of woody NPP with age is compared to the IFN plots estimates. Second, since stand age, biomass and height are correlated with each other, ORCHIDEE-FM should be able to retrieve stand age when biomass or height is assimilated. For simulations FM_{gb} and FM_{gh} where stand age is adjusted in the simulations to minimize the error on respectively biomass and height, the inferred stand age can be cross-validated by the *in situ* data on stand age.

2.4.2 Quantification of simulation improvement

2.4.2.1 Quantified evaluation criteria

To quantify the improvement in simulations resulting from the use of ORCHIDEE-FM in conjunction with external estimates of biomass or height, we focus on four carbon flux variables available in the datasets: GPP, TER, NEP, and woody NPP, this last being the indirect result of the allocation of NPP between the different organs of trees. While thirteen model evaluation criteria are computed (Appendix B) for each simulation according to the recommendations of Willmott (1982), we especially focus our analysis on two of them: the root mean square error (RMSE) as an indicator of average simulation error, and the slope of the

linear regression between simulated and measured values (*a*), as an indicator of the model's ability to reproduce a trend observed in the data.

While it is technically feasible to assimilate biomass in the standard version, as in the CASA steady-state equilibrium model (Carvalhais *et al.*, 2010), the constant mortality assumed by ORCHIDEE, and the absence of wood removals, lead to a very fast equilibrium between NPP and TER, and therefore a limited ability to take advantage of biomass data. We therefore chose to discuss directly the relative merit of ORCHIDEE-FM with biomass or height assimilation against the standard version without data assimilation.

2.4.2.2 Example of application: maps of NEP

Data-derived maps of height and volume in French forests can be obtained by a smooth interpolation of IFN data (Bellassen *et al.*, 2010b): each grid cell is attributed the averaged height and standing volume over IFN plots within a 50 km radius from its centre. In order to illustrate the potential of remote sensing data assimilation in ORCHIDEE-FM, three maps of average simulated NEP in the 1990s are then produced for France. One represents the NEP simulated by ORCHIDEE-FM without prior knowledge of the growth stage of French forests: all French forests are assumed to belong to the 40-50 years age class. The two others – one assimilating height and the other volume – show how the initial map can be refined with information on growth stage. From 15 ORCHIDEE-FM simulations over France representing stands aged between 0 and 150 years, each grid cell is attributed the NEP of the simulation with closest height or biomass to the corresponding data-derived map.

3 Results

3.1 Simulation of age-related trends by ORCHIDEE-FM

Whereas the woody NPP simulated by the standard version of ORCHIDEE is by definition insensitive to age, ORCHIDEE-FM reproduces the observed downward trend in woody NPP for both locations and both functional types

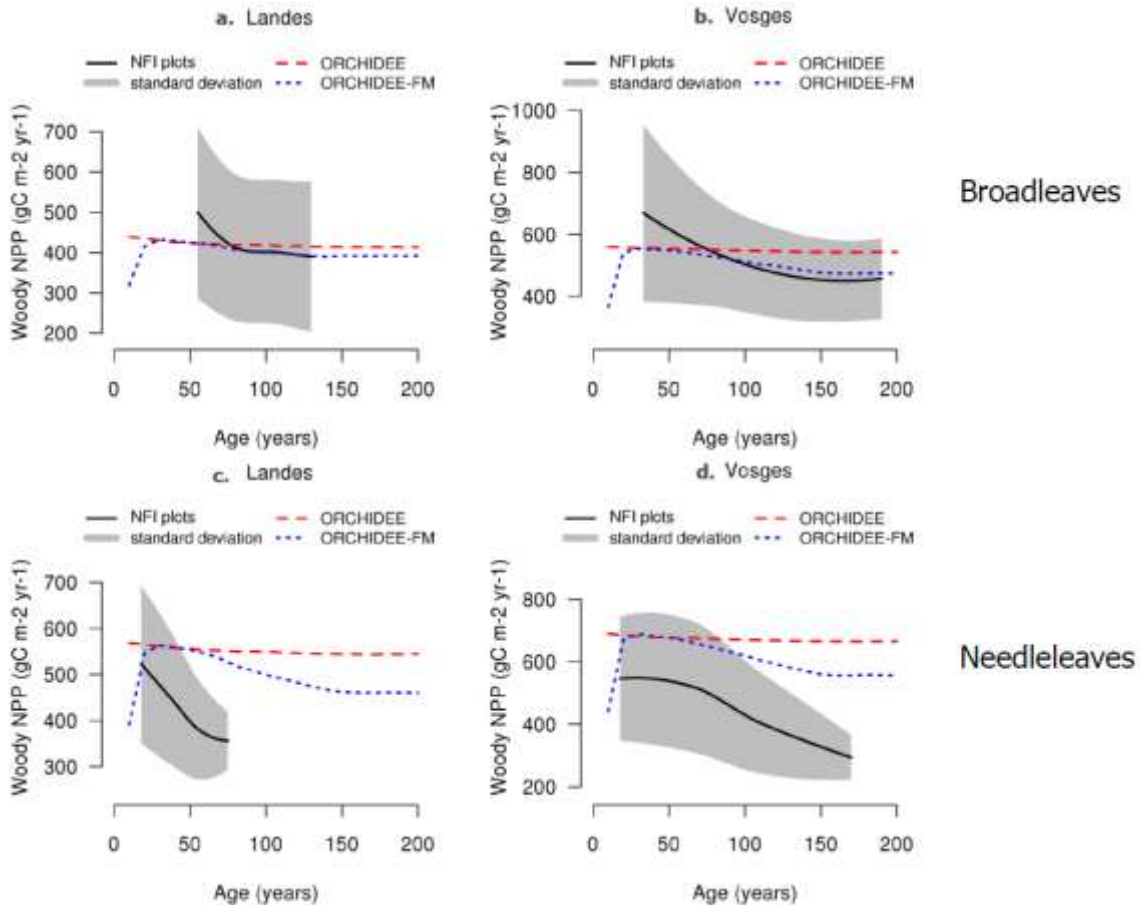

(Figure 2). The age-related decline is however steeper in IFN estimates than in simulations. In particular, the simulated decline of woody NPP is several times smaller than the standard deviation of observations for any given age class. In terms of absolute values, measured and

simulated woody NPP are comparable for broadleaves, but tend to be overestimated by the model for needleleaves.

3.2 Age retrieval from assimilation of height or biomass data

The *in situ* estimate of stand age is correctly retrieved by assimilating biomass – FM_{gb} simulation – or height – FM_{gh} simulation –for both PFTs: the shape of the frequency distribution of age differences between simulations and observations is close to a zero-centered Gaussian curve (

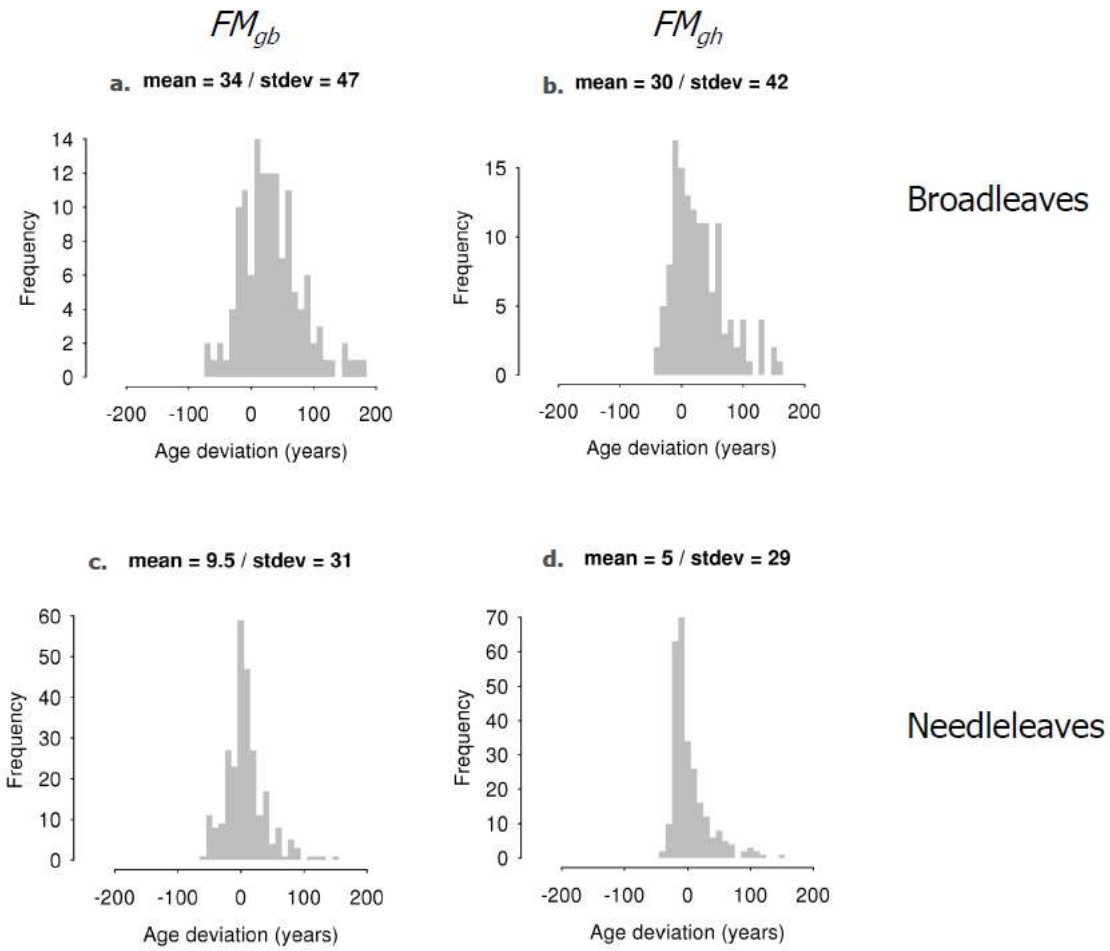

Figure 3). The spread of the distribution is larger toward positive differences, leading to a positive mean age difference of 5 to 34 years between simulations and observations, for ages measured between 10 and 250 years. This bias is comparable to the precision of the measurement (the width of measured age classes varies between 10 and 20 years). The narrower shape of height histograms indicates than assimilating average height in ORCHIDEE-FM is slightly more discriminating than assimilating biomass.

3.3 No quantified improvement in simulated woody NPP

The ability of ORCHIDEE-FM to simulate an age-related decline in woody NPP

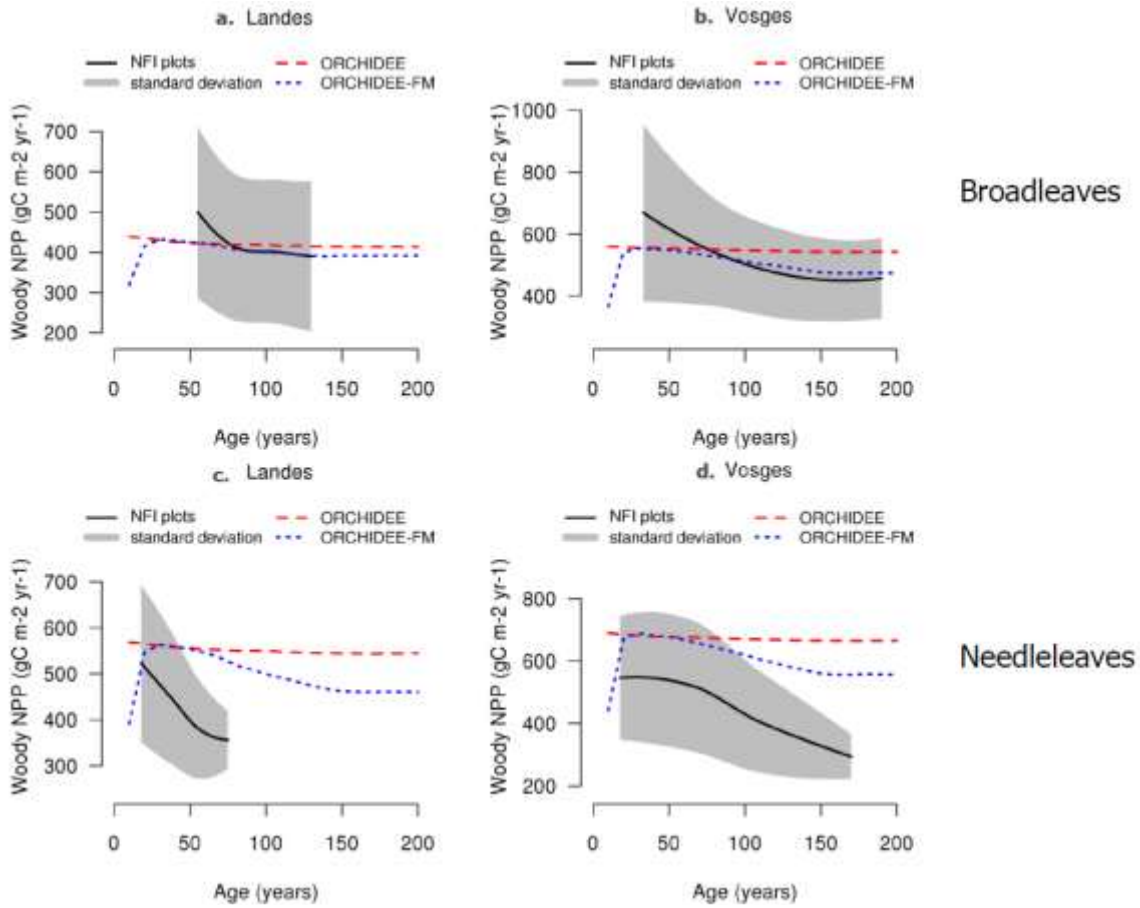

(

Figure 2) does not translate in a quantified improvement in the fit to IFN-derived estimates

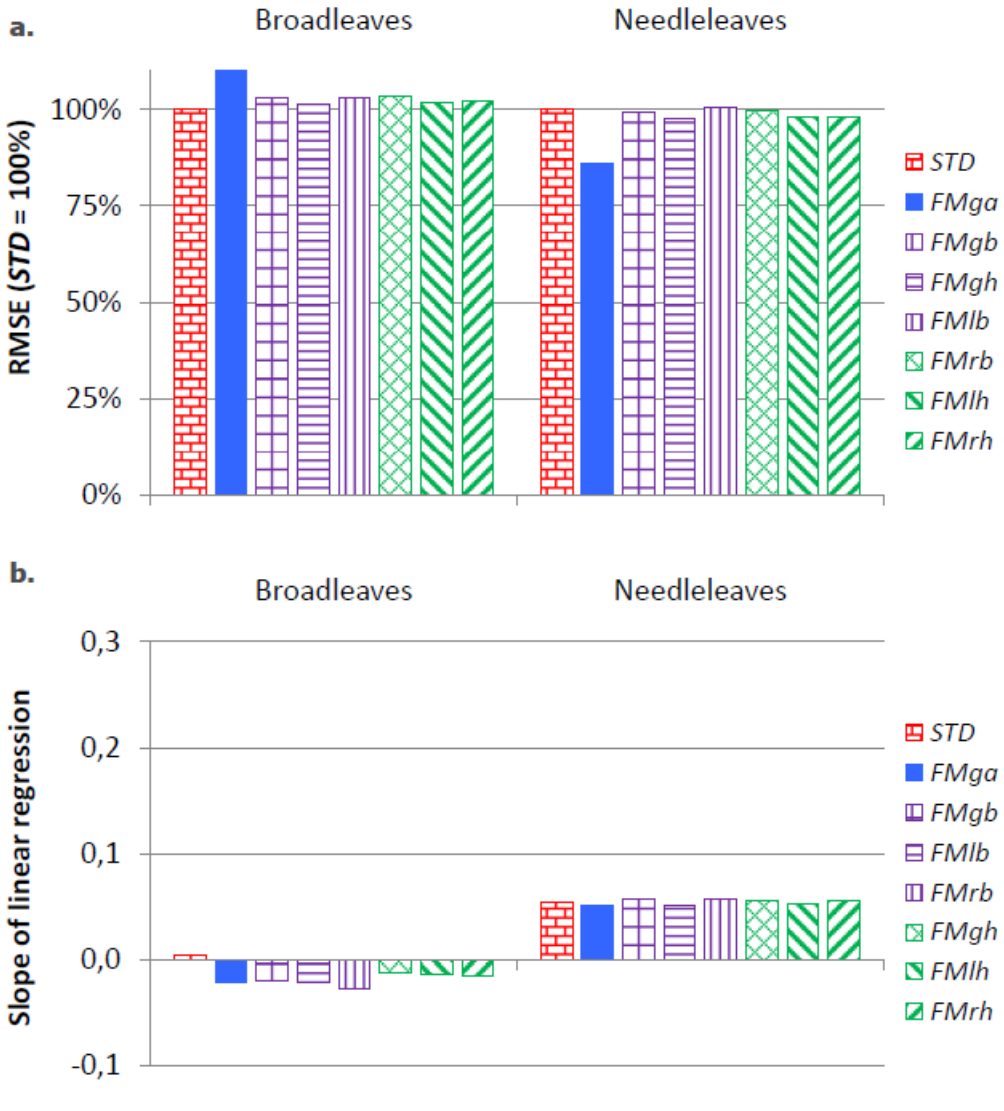

(

Figure 4): both RMSE and the slope of the linear regression are largely by model type (ORCHIDEE vs ORCHIDEE-FM) and assimilation procedure (height vs biomass, *in situ* measurement vs pseudo remote sensing data). The simulated and observed average woody NPP are comparable (Appendix C), but the models are unable to reproduce the observed cross plot variability: the slope of the linear regressions between simulations and measurements are

343 close to 0 (-0.03 – 0.6). The values of the thirteen Wilmott performance indexes are listed in
344 Appendix C.

345 *3.4 Improvement in simulated GPP, TER and NEP*

346 3.4.1 Simulation of carbon sources and sinks

347 Despite the expected presence of outliers in the global flux dataset, ORCHIDEE-FM – FM_{ga}
348 simulation – is better able than ORCHIDEE to reproduce the observed cross-sites gradient of

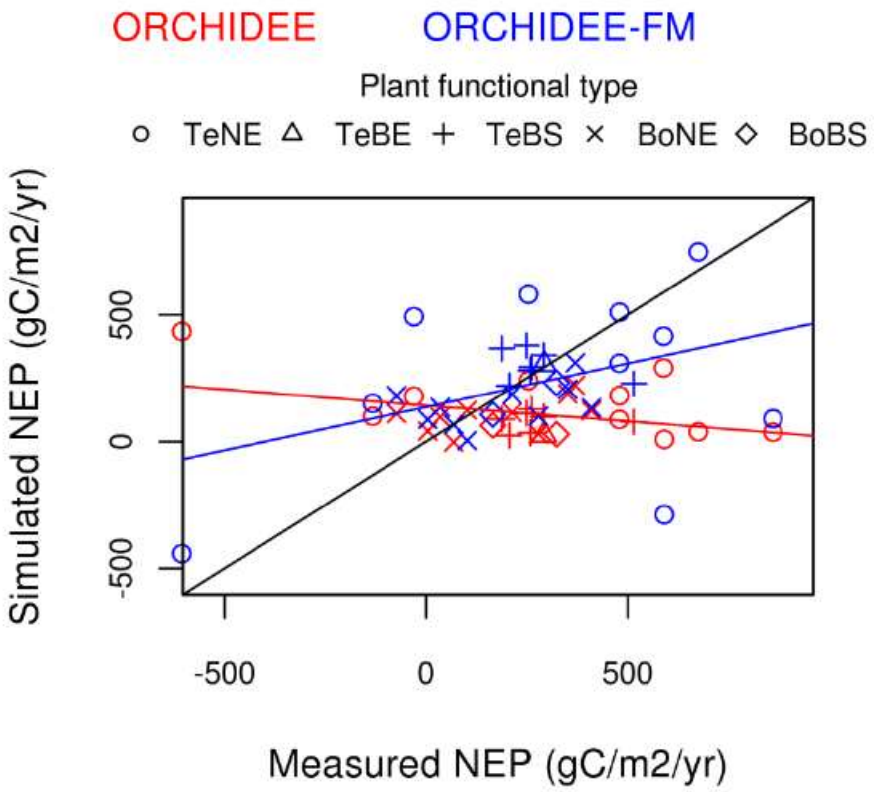

349 NEP across sites (
350 Figure 5). Interestingly, it is able to simulate the huge carbon source of -606 gC m^{-2} yr^{-1}
351 measured at the very young site of Vancouver Island.

352 The use of our "screened dataset" is justified by the exponential decrease over time of the
353 difference in simulated TER between reforested cropland and regrowing clearcut forests

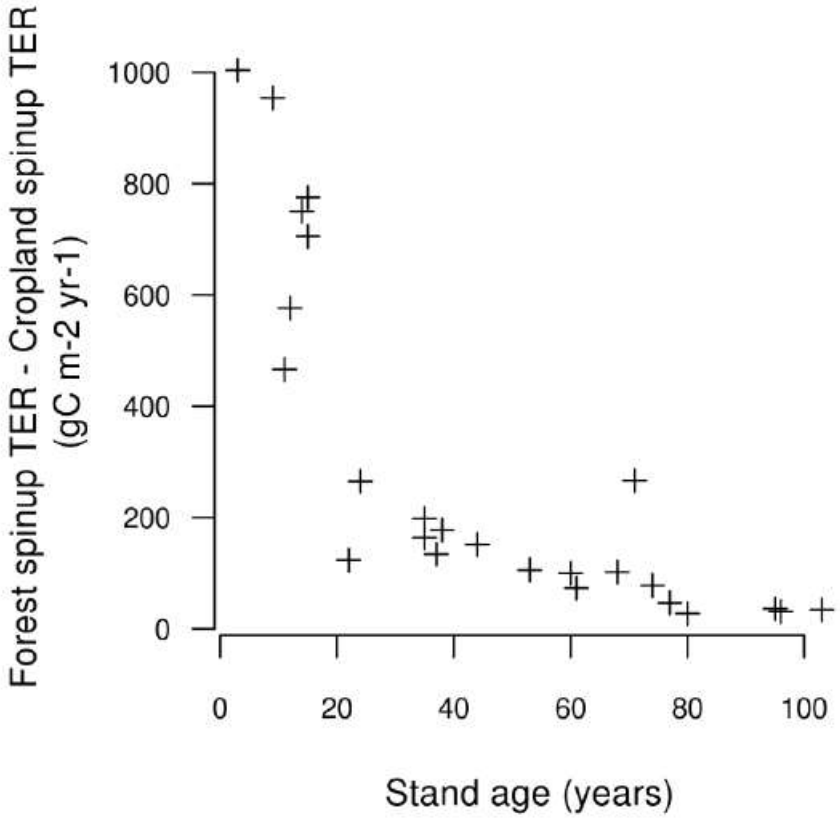

354 (
355 Figure 6). This difference can reach 1 000 gC m^{-2} yr^{-1} for younger stands but is below 300 gC m^{-2}
356 yr^{-1} for all the sites of the screened dataset, older than 20 years. These figures compare to a
357 typical simulated interannual variability of 300 gC m^{-2} yr^{-1}.

358 **3.4.2 Quantification of improvement in simulated carbon fluxes**

359 The standard version of ORCHIDEE correctly reproduces the spatial gradient of GPP across the
360 screened dataset, despite a systematic positive bias, but not that of TER (Figure 7). Due to its
361 representation of stand growth, ORCHIDEE-FM improves the simulation of TER, despite a

362 systematic positive bias, and consequently the simulation of NEP. This improvement is
363 quantified in Figure 8: the RMSE is improved (i.e. reduced) by 40-50% for TER, and by 20-40%
364 for NEP. More importantly for NEP, ORCHIDEE-FM is able to reproduce the observed variability,
365 with slopes of data-simulations linear regressions between 0.8 and 1. This is a clear
366 improvement from the NEP simulated by standard version of ORCHIDEE, which correlates very
367 poorly with observations.
368 Whereas large gross fluxes (GPP, TER) are unaffected by an additional error on pseudo remote
369 sensing data (FM_{rb}, FM_{lb}, FM_{rh} and FM_{lh} simulations), the simulation of NEP deteriorates with
370 decreasing precision of the biomass data assimilated: the assimilation of *in situ* biomass (FM_{gb})
371 improves RMSE by 37% against only 23% for pseudo-lidar biomass (FM_{lb}), and 28% for pseudo-
372 radar biomass (FM_{rb}). The slope of the linear regression is also worsened from 1.01 to
373 respectively 0.81 and 0.86.
374 Assimilating height or biomass leads to broadly similar improvements in flux simulations.
375 Biomass assimilation nevertheless seems most beneficial: while height assimilation further
376 reduces RMSE for GPP and TER, this reduction comes at the price of a degraded linear
377 regression. For NEP, biomass assimilation brings the strongest improvement in both RMSE and
378 slope of linear regression.

379 ### 3.4.3 Application: maps of NEP

380 Our simple assimilation procedure – using data-derived maps of height or biomass to select an
381 age-class in ORCHIDEE-FM simulations – produces less uniform and likely more realistic maps of
382 NEP for France (Figure 9). In particular, the older forests of central and north-eastern France are

383 detected from their higher height and biomass, leading to a lower simulated NEP than the
384 simulation without information on growth stage (Figure 9a).

385 4 Discussion

386 *4.1 Flux simulation improvement delivered by height/biomass data*

387 Our results show that a simple height or biomass data assimilation already yields a 30-50%
388 decrease in RMSE for both TER and NEP. The tested range of measurement errors (representing
389 Lidar or Radar errors) does not affect the improvement in large gross fluxes (GPP and TER).
390 However, the precision of NEP simulation is impacted: a 18.5 tC ha^{-1} uncertainty on the
391 assimilated biomass data, typical of P-band radar measurements, increases the simulation error
392 by 20 gC m^2 yr^{-1} (7.5% of observed average NEP), and a 23.6 tC ha^{-1} uncertainty, typical of LiDAR
393 derived estimates, increases the simulation error by 31 gC m^2 yr^{-1} (11.5% of observed average
394 NEP). Thus, a reduced error on remote sensing estimates of biomass would not be useful for
395 the simulation of large fluxes, but could further reduce the error on simulated NEP by 20-31 gC
396 m^2 yr^{-1} down to 149 gC m^2 yr^{-1}, that is the error obtained by assimilating the i*n situ* estimate.

These results are both site- and model-dependent. For instance, the strong influence of land-use history on the NEP of younger stands limits the benefits of the assimilation procedure

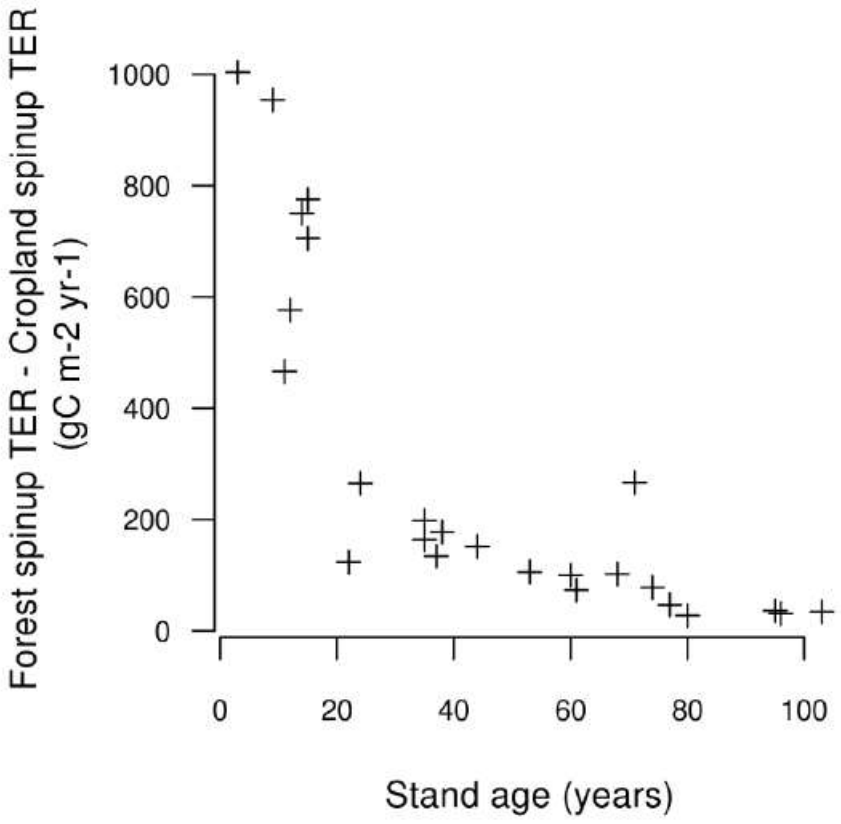

(

Figure 6). More elaborate distinctions in the usefulness of the method could possibly be made based on PFT or climate, but the small size of the screened dataset does not allow to draw robust conclusions.

The error reduction in simulated fluxes could also be further improved by improvements in the structure and in the parameterisation of ORCHIDEE-FM. In particular, our results point to systematic positive biases in the simulation of GPP and TER which offset one another in the simulation of NEP. Zaehle *et al.* (2010) demonstrated that modelling the nitrogen cycle

407 eliminates this systematic bias. This new version of ORCHIDEE, ORCHIDEE-N, remains however
408 unable to simulate the large positive NEP typical of growing forest sites. In the near future,
409 when ORCHIDEE-FM is merged with ORCHIDEE-N, we can expect to reduce the bias in GPP and
410 TER, and further decrease the error on NEP by assimilating age, height or biomass.

411 Our assumption that remote sensing measurement error is independent on measured value
412 and normally distributed is not realistic. Remote sensing measurements of biomass for example
413 are known to carry a larger error for larger biomass values due to signal saturation (Le Toan *et*
414 *al.*, 2008). We nevertheless opted for this simplistic approach of error modelling due to the lack
415 of quantification of these error patterns. An alternative to improving error modelling would be
416 to use real remote sensing data where it coincides with *in situ* measurements of carbon fluxes,
417 but this additional requirement would further reduce an already small dataset.

418 The simple data assimilation framework tested in this study could easily be applied at
419 continental scale, provided reliable biomass or height estimates are available. It would be most
420 meaningful in temperate and boreal regions, where carbon fluxes are most impacted by
421 management and age effects (Grant *et al.*, 2007; Magnani *et al.*, 2007; Nunery and Keeton,
422 2010): most temperate forests are thinned or harvested, and large fires are the dominant
423 source of disturbance in boreal forests.

424 These large-scale applications are very promising: TER is the component of NEP for which
425 existing GVM estimates are most uncertain (Mitchell *et al.*, 2009), and it is also the flux for
426 which simulation improvement is largest in our framework. This large improvement in TER
427 comes from the process-based mortality and wood removals simulated by ORCHIDEE-FM. For a

test broadleaf site in northeastern France, Bellassen *et al.* (2010a) showed that the delay in litterfall and the wood removals were responsible for 60% and 40% of the sink over one forest rotation respectively. The combination of these two processes allows the simulation of a realistic disequilibrium in biomass and soil carbon.

4.2 Scale issues in spatial heterogeneity

The ability of ORCHIDEE-FM to simulate correctly the across-site gradient in "growth stages" of the global flux dataset does not yield a quantitative improvement in the simulation of woody NPP for the IFN dataset. This difference points out the limits in the notion of "growth stage". While it applies relatively well to some characteristics such as NEP (these characteristics evolving similarly in all stands, albeit not at the same pace), other variables such as woody NPP cannot be easily explained in this light only. Forests standing on poor soils for example will never have strong woody NPP, no matter how long one waits. As illustrated in Figure 10, the large variability in woody NPP for stands of similar ages highlights the importance of other factors than growth stage: the growth stage-dependent allocation and photosynthesis efficiency simulated in ORCHIDEE-FM cannot be expected to reproduce such a wide range of observed values.

444 The same phenomenon explains that the spread of age deviation distributions presented in

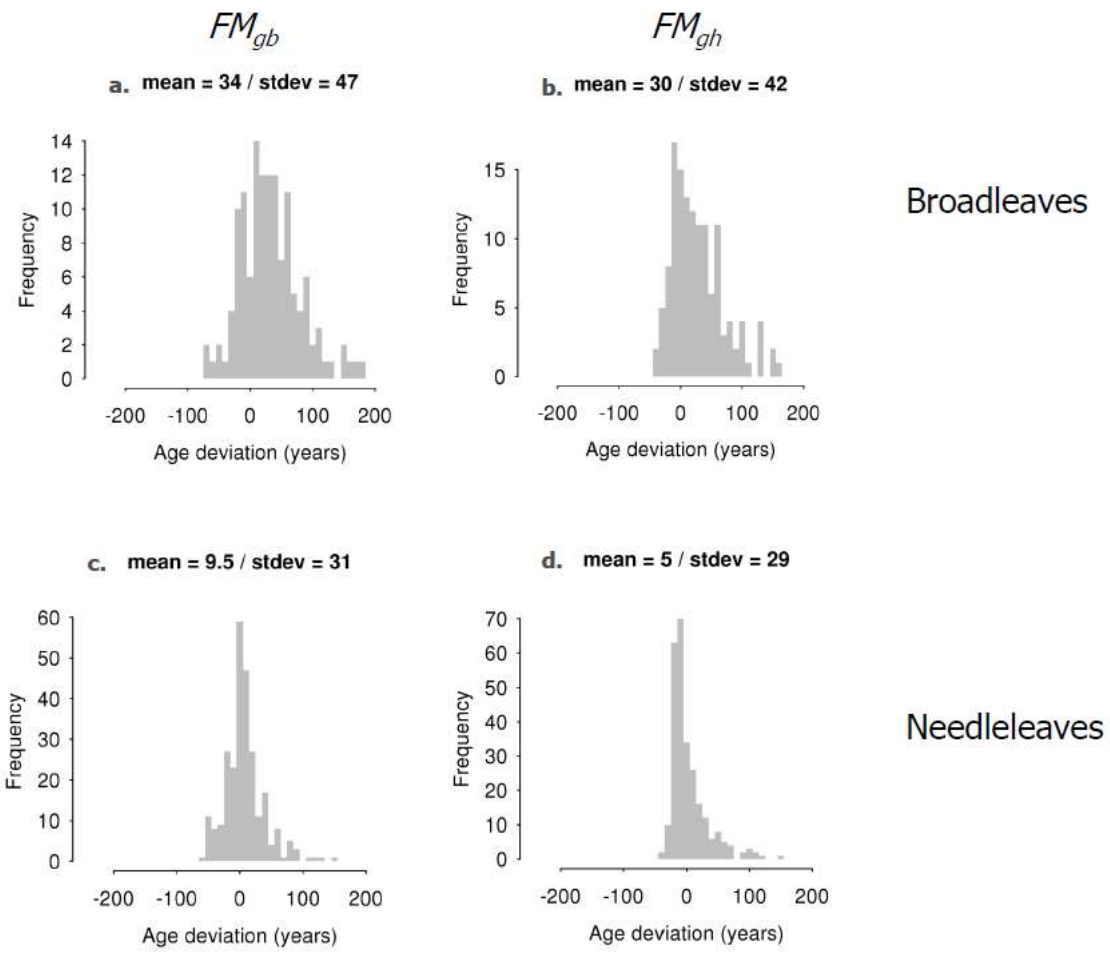

445

446 Figure 3 is larger on the positive (younger ages) than on the negative (older ages) side. The
447 assimilation framework can go very far towards younger simulated ages in order to match a
448 small observed biomass, but the reverse is not true for high observed biomass: the old stands
449 of average productivity simulated by ORCHIDEE-FM cannot reach the biomass of some
450 observed high productive stands which are only slightly younger.

451 This large residual heterogeneity is most likely explained by species or local fertility, which
452 could also be integrated in ORCHIDEE-FM. Model parameters in particular could be adapted to

distinguish between fast-growing and slow-growing species. The main limitation for these developments is the ability to get proxies for these factors on a large scale. Fine resolution maps of species or site productivity are even more difficult to obtain than equivalent maps of height or biomass, although they may not be completely unmanageable (Nabuurs *et al.*, 2008).

4.3 Biomass vs. height

The application of our method on the global flux dataset points to biomass as a more suitable candidate than average height for assimilation in ORCHIDEE-FM. The smaller RMSE obtained for GPP and TER in the FM_{gh}, FM_{lh}, and FM_{rh} simulations are indeed misleading. They result from an overestimate of stand age which activates age-related decline processes in ORCHIDEE-FM: while the previously discussed positive biases in GPP and TER are consequently reduced, they are probably not reduced for the correct reason since the RMSE in NEP is higher than for the FM_{gb} simulation. As shown by Figure 11, the assimilation of height in ORCHIDEE-FM indeed leads to an overestimate of stand age for other plant functional types than temperate summergreen broadleaves and temperate evergreen needleleaves. This overestimate probably comes from the height-circumference allometry and the self-thinning relationship of ORCHIDEE-FM, which have only been tested rigorously for temperate summergreen broadleaves and temperate evergreen needleaves.

The IFN dataset, which is restricted to these two plant functional types, provides a different picture. The narrower and more centered distributions of age deviation for FM_{gh} simulations

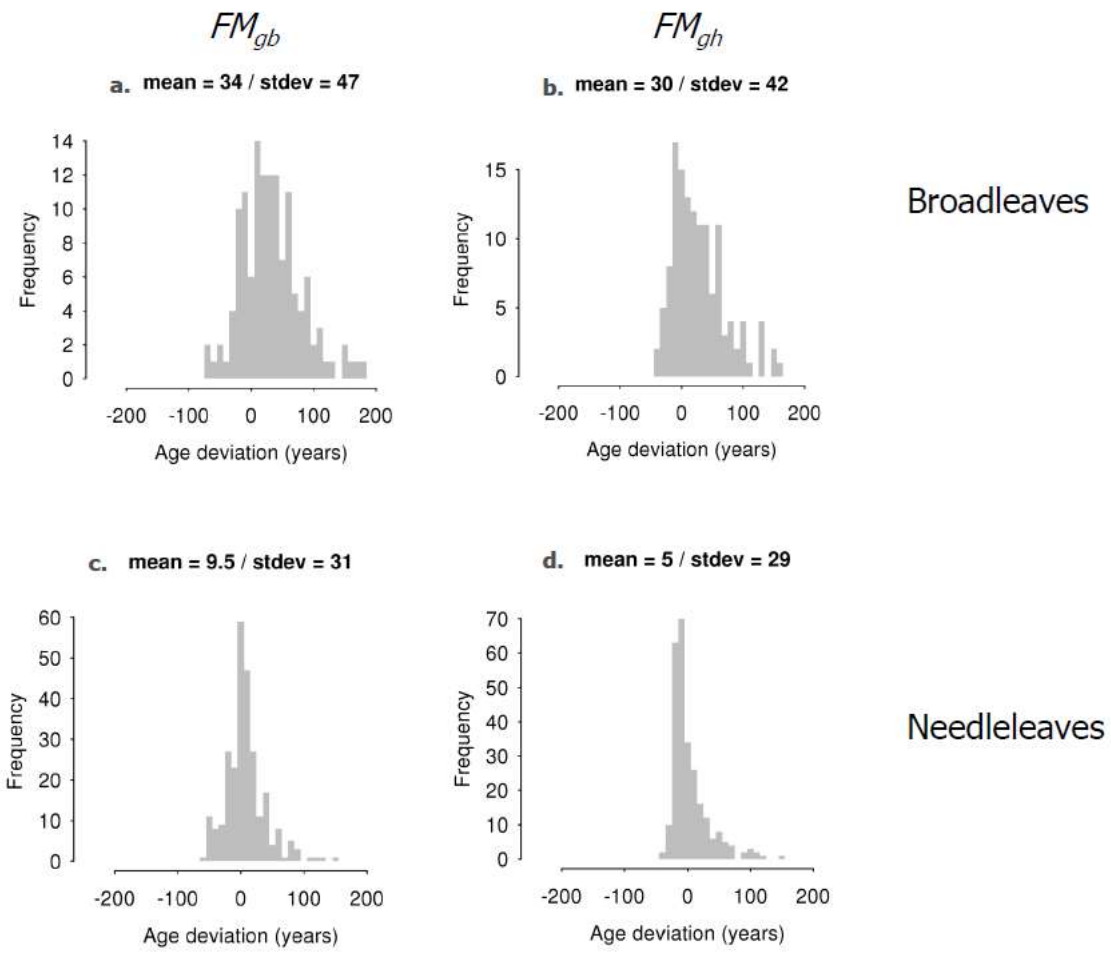

(see Figure 3) point to height as a more useful variable for assimilation in ORCHIDEE-FM. Height is indeed expected to be less sensitive than biomass to varying intensities of management.

These contradicting results make it difficult to draw a general and definitive conclusion on the relative merits of height vs. biomass assimilation in ORCHIDEE-FM. While height seems theoretically more promising, the allometric and self-thinning rules of ORCHIDEE-FM may not be currently generic enough to make the best use of it.

4.4 Retrieval of unmeasured variables

Some variables, such as stand age or soil carbon content, are difficult to measure and therefore seldom available at a fine resolution over large areas. Ours results show that ORCHIDEE-FM is able to use biomass or height data, in addition to pedo-climatic conditions, to correctly retrieve stand age. If such data were available over large areas, this simple assimilation method could therefore produce a new set of stand age maps. The method is independent of the combination of inventory data and remote sensing of disturbances used by Pan *et al.* (2010) to produce age maps over north America, and the disagreements between the two would undoubtedly provide useful insights on the strengths and weaknesses of both methods.

Estimates of soil carbon content could also be retrieved from ORCHIDEE-FM by assimilating simultaneously biomass and NEP. Assuming that the model simulates correctly NPP and litterfall once it has been initialised for biomass, the resulting discrepancy between measured and simulated NEP would be due to a faulty soil carbon content, which could then be corrected in the model to match the NEP measurements.

5 Conclusion

Large-scale information on biomass derived from remote sensing estimates would provide valuable constraints for the simulation of carbon fluxes in ORCHIDEE-FM: the RMSE of simulated NEP is decreased by up to 30% for a global flux dataset. Most importantly, this improvement results from the ability of ORCHIDEE-FM, initialized with the correct “growth

498 stage", to reproduce spatial gradients in NEP, an ability that is lacking in the standard steady-
499 state equilibrium version of ORCHIDEE.
500 At a smaller spatial scale, where climate conditions are comparable, remotely sensed
501 information on "growth stage" does not bring a useful constraint on woody NPP, probably
502 because of the relatively higher importance of local factors such as soil fertility and species mix.
503 The notion of "growth stage" may also be less relevant for woody NPP than for NEP.
504 Nevertheless, our simple assimilation framework for height or biomass correctly retrieves stand
505 age, despite a large standard deviation.
506 The simulated error of pseudo remote sensing estimates of biomass or height does not impact
507 the improvement of large gross fluxes (GPP and TER). For simulated NEP however, this
508 additional source of uncertainty increases the total error by 13.5% and 21% for P-band radar
509 and lidar respectively.
510 Finally, while the results of our simple assimilation framework are promising, they represent
511 only a first assessment of the potential of large-scale data assimilation in DGVMs. New
512 developments in ORCHIDEE (Zaehle and Friend, 2010), and more refined assimilation
513 frameworks, including other remotely sensed variables such as leaf area index (Demarty *et al.*,
514 2007) or CO_2 concentration (Sarrat *et al.*, 2009), will doubtlessly optimize the use that
515 ORCHIDEE-FM can make of remote sensing estimates of biomass and height.

516 ## Acknowledgements

517 We want to acknowledge the contribution of Antoine Colin (IFN), without whom the work on
518 the dataset he manages would have been both impossible and meaningless. We also

519 appreciated the expert comments of Thuy Le Toan (CESBIO) and Patrick Chazette (LSCE) on
520 remote sensing estimates.

521 This work was made possible thanks to a research grant from the French ministry for research.

522

Appendixes

Appendix A. Subsample of the global carbon flux dataset (Luyssaert *et al.*, 2007) used in this study ("global flux dataset")

ID	Site name	Latitude	Longitude	PFT[1]	ASH[2] (m)	Biomass (gC m-2)	GPP (gC m^{-2} yr^{-1})	RECO (gC m^{-2} yr^{-1})	NEP (gC m^{-2} yr^{-1})	YE[3]	ME[4]	Age (years)
1003	Collelongo	41.75 °N	13.75 °E	TeBS	19.0	9 860	1 127	591	583	1895	1998	103
1004	Prince_Albert_SSA_(SOAS)	53.75 °N	106.25 °W	BoBS	20.3	1 997	1 215	1 030	178	1928	1998	70
1006	Prince_Albert_SSA_(SOJP)	53.75 °N	104.75 °W	BoNE	13.0	1 997	690	638	35	1931	1999	68
1007	Thompson_NSA_(NYJP)	55.75 °N	98.25 °W	BoNE	5.0	3 090	960	550	410	1972	1994	22
1012	Bayreuth/Weiden_Brunnen	50.25 °N	11.75 °E	TeNE	36.0	9 267	1 303	1 334	-32	1954	1998	44
1014	Slash_pine_Florida_Mid	29.75 °N	82.25 °W	TeNE	10.0	2 285	2 762	2 087	589	1987	1999	12
1015	Slash_pine_Florida_old	29.75 °N	82.25 °W	TeNE	19.0	8 271	2 606	1 944	675	1973	1998	25
1089	Duke_Forest	35.75 °N	79.25 °W	TeNE	14.0	5 128	1 788	1 233	497	1982	2000	18
1092	Harvard	42.75 °N	72.25 °W	TeBS	25.0	9 900	1 287	1 058	202	1936	1997	61
1093	Walker_Branch	35.75 °N	84.25 °W	TeBS	25.3	5 715	1 690	1 335	514	1930	1997	67
1095	Flakaliden_C	64.25 °N	19.25 °E	BoNE	4.7	1 770	1 000	932	104	1960	2000	40
1096	Norunda	60.25 °N	17.25 °E	BoNE	28.0	11 135	1 312	1 404	-61	1900	1999	99
1097	Hyytiala	61.75 °N	24.25 °E	BoNE	15.5	5 900	1 012	782	233	1964	2000	36
1101	Willow_Creek	45.25 °N	90.25 °W	BoBS	24.0	7 490	1 165	835	289	1933	1999	66
1106	Morgan_Monroe	39.25 °N	86.25 °W	TeBS	26.5	8 720	1 452	1 163	279	1924	2000	76
1109	Le_Bray	44.75 °N	0.75 °W	TeNE	19.0	7 008	1 833	1 451	407	1969	2000	31
1110	Balmoral	42.75 °S	172.75 °E	TeNE	8.0	3 700	1 774	1 166	608	1987	1996	9
1154	Oak_ridge_liriodendron	35.75 °N	84.25 °W	TeBS	30.0	6 288	na	na	249	1918	2000	82
1168	Skyttorp2	60.25 °N	17.75 °E	BoNE	16.0	6 063	1 232	953	360	1970	2004	34
1169	Puechabon	43.75 °N	3.75 °E	TeBE	6.0	5 424	1 379	1 071	309	1942	2002	60
1170	Dooary	52.75 °N	7.25 °W	TeNE	8.0	6 162	2 001	1 141	860	1989	2004	15
1178	Takayama	36.25 °N	137.25 °E	TeBS	20.0	13 488	1 050	833	217	1962	1997	35
1185	Hyytiala_12	61.75 °N	24.25 °E	BoNE	4.0	250	854	752	102	1991	2002	11
1246	Hyytiala_75	61.75 °N	24.25 °E	BoNE	25.0	6 700	918	566	352	1927	2001	74
1328	Skyttorp3	60.25 °N	17.75 °E	BoNE	18.0	7 310	na	na	370	1938	2002	64
1364	Espirra	38.75 °N	8.75 °W	TeBE	20.0	4 212	1 495	876	619	1991	2004	13
1378	Bartlett	44.25 °N	71.25 °W	TeBS	19.0	10 730	1 053	790	263	1925	2005	80
1482	Chibougamau_EOBS	49.75 °N	74.25 °W	BoNE	14.0	4 500	584	580	4	1909	2004	95
1507	Vancouver_Island_HDF00	49.75 °N	125.25 °W	TeNE	1.0	2 775	435	1 041	-606	1999	2002	3
1508	Vancouver_Island_HDF88	49.75 °N	124.75 °W	TeNE	8.0	5 700	1 214	1 347	-133	1988	2002	14
1509	Vancouver_Island_DF49	49.75 °N	125.25 °W	TeNE	29.0	10 550	1 991	1 737	337	1949	2001	52

1. TeNE: tempereate needleleaf evergreen, TeBE: temperate broadleaf evergreen, TeBS: temperate broadleaf summergreen, BoNE: boreal needleleaf evergreen, BoBS: boreal broadleaf summergreen

2. Average stand height / 2. Year of establishment / 3. Measurement year

528 Appendix B. Wilmott performance indexes (Willmott, 1982)

Index	Name	Equation
OA	Average value of observations	$\frac{1}{N}\sum_i O_i$
SA	Average value of simulations	$\frac{1}{N}\sum_i S_i$
OS	Standard deviation of observations	$\frac{1}{N-1}\sum_i (O_i - OA)$
SS	Standard deviation of simulations	$\frac{1}{N-1}\sum_i (S_i - SA)$
N	Number of observations	
a	Slope of linear regression (simulations = f(observations))	
b	Intercept of linear regression (simulations = f(observations))	
MAE	Mean absolute error	$\frac{1}{N}\sum_i \lvert S_i - O_i \rvert$
RMSE	Root mean square error	$\sqrt{\frac{1}{N}\sum_i (S_i - O_i)^2}$
RMSEs	Systematic root mean square error	$\sqrt{\frac{1}{N}\sum_i (O_i - P_i)^2}$
RMSEu	Unsystematic root mean square error	$\sqrt{\frac{1}{N}\sum_i (S_i - P_i)^2}$
d	Index of agreement	$1 - \frac{\sum_i (S_i - O_i)^2}{\sum_i (\lvert S_i - OA \rvert + \lvert O_i - OA \rvert)^2}$
r^2	Square of Pearson's correlation coefficient	$\frac{\sum_i (S_i - SA)(O_i - OA)}{\sqrt{\sum_i (S_i - SA)^2} \times \sqrt{\sum_i (O_i - OA)^2}}$

$S_{1..N}$ are the N simulate values, $O_{1..N}$ are the N measured values, and $P_{1..N}$ are the values predicted by the linear regression: $\forall i, P_i = aO_i + b$

529

530 Appendix C. Wilmott performance indexes for the simulation of volume increment (IFN dataset)

531 Abbreviations for the names of performance indexes are given in Appendix B. For details on

532 simulations names, see part 2.3.2, Appendix E and

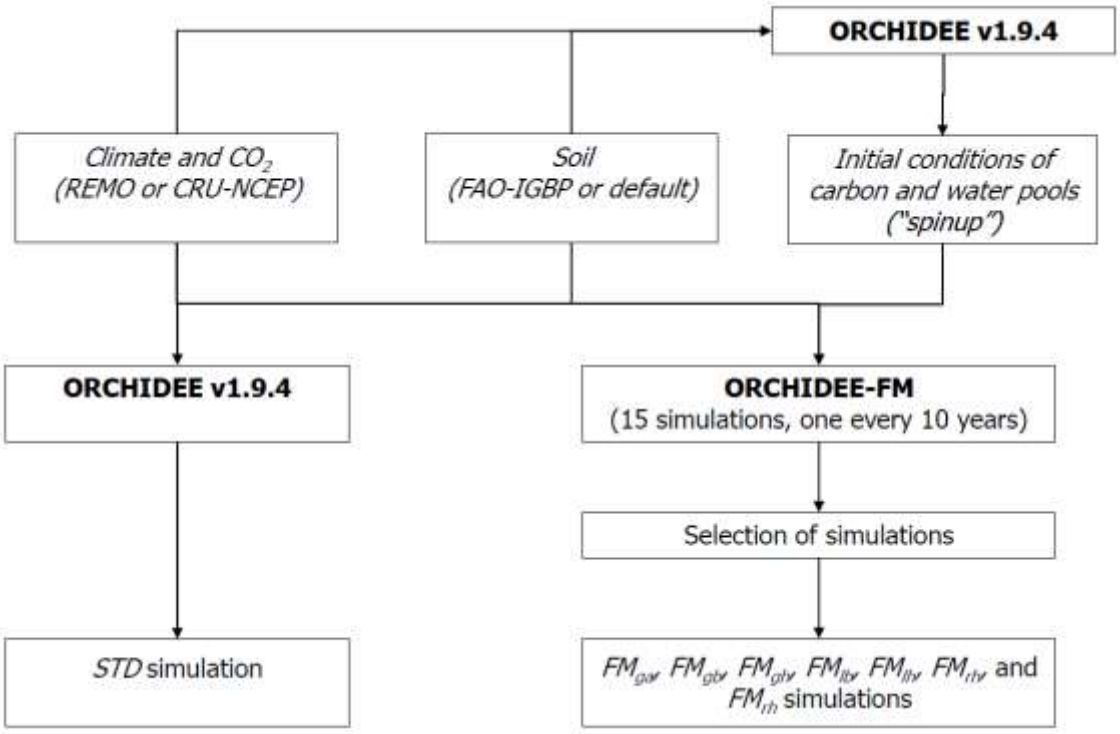

533

534 Figure 1.

Woody NPP - broadleaves (gC m^{-2} yr^{-1})													
Simulation	obs average	sim average	obs sd	sim sd	N	a	b	MAE	RMSE	RMSEs	RMSEu	d	r2
STD	426.7	520.7	241.9	55.5	211	0.00	518.81	214.0	263.8	258.0	55.4	0.36	0.00
FM_{ga}	468.9	523.4	280.5	41.3	86	-0.02	533.51	234.1	292.9	290.1	40.6	0.20	0.02
FM_{gb}	426.7	534.1	241.9	38.6	211	-0.02	543.00	221.5	271.4	268.7	38.2	0.35	0.02
FM_{gh}	426.7	530.2	241.9	37.6	211	-0.01	535.58	219.3	268.0	265.4	37.4	0.34	0.01
FM_{lb}	426.7	536.2	241.9	37.5	211	-0.02	545.14	222.9	272.1	269.6	37.1	0.35	0.02
FM_{rb}	426.7	533.8	241.9	39.0	211	-0.03	545.63	223.8	272.8	270.1	38.3	0.34	0.03
FM_{lh}	426.7	530.1	241.9	38.5	211	-0.01	536.03	219.3	268.3	265.6	38.3	0.34	0.01
FM_{rh}	426.7	531.9	241.9	38.2	211	-0.02	538.57	220.2	269.4	266.7	37.9	0.34	0.01

535

Woody NPP - needleleaves (gC m^{-2} yr^{-1})													
Simulation	obs average	sim average	obs sd	sim sd	N	a	b	MAE	RMSE	RMSEs	RMSEu	d	r2
STD	481.5	650.9	219.1	71.0	328	0.05	624.71	228.4	276.4	267.4	69.9	0.48	0.03
FM_{ga}	483.1	617.1	193.8	70.4	172	0.05	592.82	189.1	237.7	227.3	69.5	0.46	0.02
FM_{gb}	481.5	648.2	219.1	72.8	328	0.06	620.94	225.2	274.8	265.3	71.6	0.48	0.03
FM_{gh}	481.5	640.5	219.1	70.8	328	0.06	613.97	220.6	269.9	260.8	69.7	0.48	0.03
FM_{lb}	481.5	651.6	219.1	71.6	328	0.05	627.34	227.3	277.6	268.5	70.7	0.48	0.02
FM_{rb}	481.5	649.4	219.1	72.7	328	0.06	621.86	225.0	275.4	265.9	71.5	0.48	0.03
FM_{lh}	481.5	642.1	219.1	71.1	328	0.05	616.99	222.3	271.5	262.3	70.0	0.47	0.03
FM_{rh}	481.5	641.8	219.1	70.6	328	0.06	615.26	220.7	270.6	261.6	69.4	0.48	0.03

536

537

538 Appendix D. Wilmott performance indexes for the simulation of GPP, TER and NPP (screened
539 global flux dataset)

540 Abbreviations for the names of performance indexes are given in Appendix B. For details on
541 simulations names, see part 2.3.2, Appendix E and

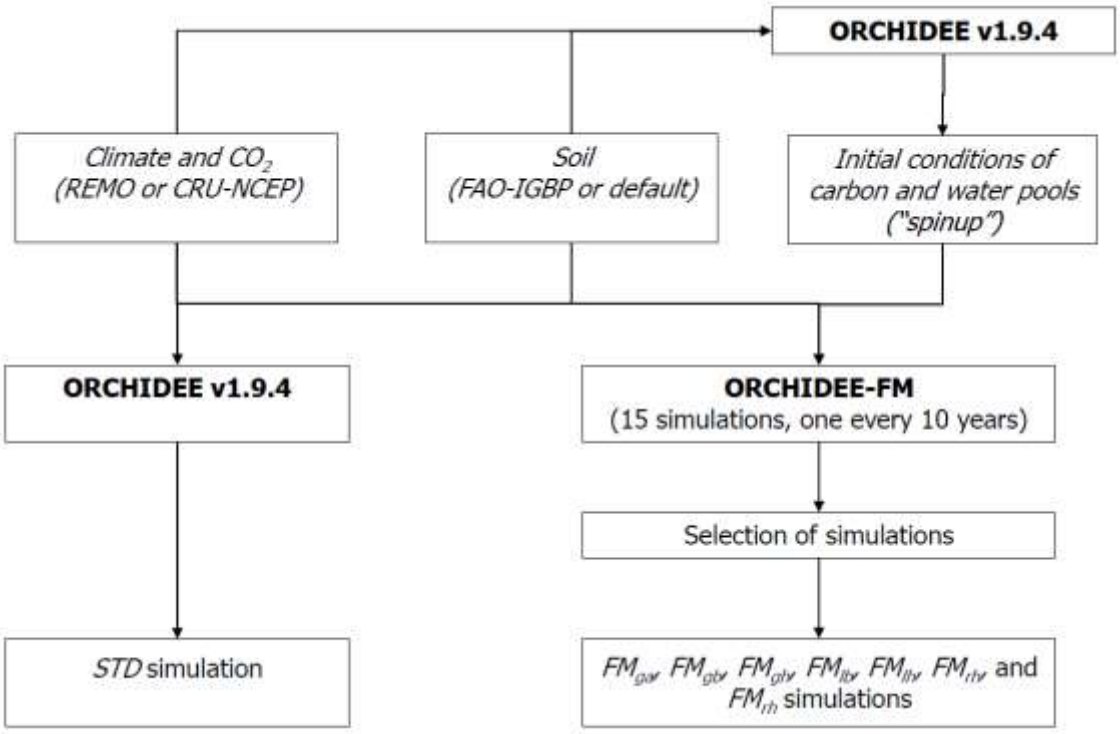

542

543 Figure 1.

GPP (gC m^{-2} yr^{-1})	OA	SA	OS	SS	N	a	b	MAE	RMSE	RMSEs	RMSEu	d	r2
STD	1296	1579	502	582	18	1.12	129	286	325	289	149	0.91	0.93
FM_{ga}	1296	1562	502	593	18	1.14	87	269	315	274	154	0.92	0.93
FM_{gb}	1296	1562	502	601	18	1.15	71	279	319	276	160	0.92	0.92
FM_{gh}	1296	1472	502	613	18	1.15	-22	219	274	190	197	0.94	0.89
FM_{lb}	1296	1544	502	596	18	1.13	73	269	310	258	167	0.92	0.91
FM_{rb}	1296	1552	502	597	18	1.14	75	273	313	265	164	0.92	0.92
FM_{lh}	1296	1475	502	619	18	1.17	-43	219	272	198	185	0.94	0.90
FM_{rh}	1296	1475	502	620	18	1.17	-45	220	272	198	185	0.94	0.90

TER (gC m^{-2} yr^{-1})	OA	SA	OS	SS	N	a	b	MAE	RMSE	RMSEs	RMSEu	d	r2
STD	1032	1493	403	569	18	1.31	142	462	520	477	207	0.76	0.86
FM_{ga}	1032	1288	403	425	18	0.96	302	263	311	257	176	0.86	0.82
FM_{gb}	1032	1324	403	423	18	0.96	333	292	336	292	166	0.85	0.84
FM_{gh}	1032	1269	403	412	18	0.94	296	250	285	239	156	0.88	0.85
FM_{lb}	1032	1331	403	443	18	0.99	310	301	354	301	187	0.84	0.81
FM_{rb}	1032	1330	403	436	18	0.98	321	300	350	299	183	0.84	0.82
FM_{lh}	1032	1262	403	416	18	0.95	278	241	278	231	155	0.89	0.85
FM_{rh}	1032	1261	403	416	18	0.95	277	241	278	230	155	0.89	0.85

NEP (gC m^{-2} yr^{-1})	OA	SA	OS	SS	N	a	b	MAE	RMSE	RMSEs	RMSEu	d	r2
STD	269	94	152	70	20	0.12	62	185	229	219	66	0.46	0.06
FM_{ga}	269	282	152	176	20	0.79	69	97	129	34	125	0.82	0.47
FM_{gb}	269	250	152	214	20	0.99	-17	110	149	19	148	0.81	0.50
FM_{gh}	269	213	152	255	20	0.98	-49	155	210	56	202	0.70	0.34
FM_{lb}	269	226	152	215	20	0.79	15	134	180	59	163	0.74	0.40
FM_{rb}	269	235	152	212	20	0.84	10	127	169	47	158	0.76	0.42
FM_{lh}	269	223	152	244	20	0.96	-34	146	194	47	189	0.73	0.37
FM_{rh}	269	223	152	244	20	0.96	-34	146	194	47	188	0.73	0.37

Appendix E. Abbreviations

5.1.1.1.1.1 General terms

FMM: Forest Management Module

GPP: Gross Primary Productivity

GVM: Global Vegetation Model

IFN: French National Forest Inventory

NEP: Net Ecosystem Productivity (a positive value indicates a carbon sink)

NPP: Net Primary Productivity

PFT: Plant Functional Type

RMSE: Root Mean Square Error

TER: Terrestrial Ecosystem Respiration

5.1.1.1.1.2 Simulations names

STD: Simulation using the standard version of ORCHIDEE, representing a forest stand at steady-state equilibrium.

FM_{ga}: Simulation with closest age to the *in situ* estimate, selected from a set of ORCHIDEE-FM simulations separated by 10-years intervals.

FM_{gb}: Simulation with closest biomass to the *in situ* estimate, selected from a set of ORCHIDEE-FM simulations separated by 10-years intervals.

FM_{gh}: Simulation with closest average stand height to the *in situ* estimate, selected from a set of ORCHIDEE-FM simulations separated by 10-years intervals.

567 FM_{lb}: Simulation with closest biomass to the pseudo-lidar estimate, selected from a set of
568 ORCHIDEE-FM simulations separated by 10-years intervals.
569 FM_{rb}: Simulation with closest biomass to the pseudo-radar estimate, selected from a set of
570 ORCHIDEE-FM simulations separated by 10-years intervals.
571 FM_{lh}: Simulation with closest average stand height to the pseudo-lidar estimate, selected from
572 a set of ORCHIDEE-FM simulations separated by 10-years intervals.
573 FM_{rh}: Simulation with closest average stand height to the pseudo-radar estimate, selected from
574 a set of ORCHIDEE-FM simulations separated by 10-years intervals.
575

576 # Tables

Parameter	Conifers	Broadleaves	Unit	Source
BEF_i	1.1	1.2	no unit	(IPCC, 2003)
T_b	0.025	0.025	yr^{-1}	(Bellassen *et al.*, 2010a)
br	0.25	0.38	no unit	(Bellassen *et al.*, 2010a)
d_c	0.5	0.5	gC gDM^{-1}	(Bellassen *et al.*, 2010a)
d_w	$0.4*10^6$	$0.6*10^6$	gDM m^{-3}	(Bellassen *et al.*, 2010a)

577

578 Table 1. Parameter values

579

Name	Landes	Vosges
Latitude	43.875°N	48.125°N
Longitude	0.875°W	6.875°E
2001-2005 average temperature (°C)	14.3	9.7
2001-2005 average rainfall (mm yr^{-1})	925	971
Number of broadleaf plots within a 0.5° radius	78	133
Number of needleleaf plots within a 0.5° radius	137	191
Average volume increment of neighbouring broadleaf plots (m^3 ha^{-1})	12.2	14.0
Average volume increment of neighbouring needleleaf plots (m^3 ha^{-1})	19.8	22.2
Average age of neighbouring broadleaf plots (years)	92	97
Average age of neighbouring needleleaf plots (years)	42	71

580

581 Table 2. Description of the IFN plots used in this study

Remote sensing technique	LiDAR (airborne)	P-band RADAR (airborne)
Average stand height		
RMSE (m)	1.66	2.34
Number of studies	5	3
References	(Nelson *et al.*, 2003; Balzter *et al.*, 2007a; Balzter *et al.*, 2007b; Stephens *et al.*, 2007; Breidenbach *et al.*, 2008)	(Neeff *et al.*, 2005; Dubois-Fernandez *et al.*, 2008; Hajnsek *et al.*, 2009)
Aboveground biomass		
RMSE (tC ha^{-1})	23.66	18.5
Number of studies	9	6
References	(Means *et al.*, 1999; Drake *et al.*, 2002; Lim and Treitz, 2004; Lefsky *et al.*, 2005b; Watt and Haywood, 2006; Hyde *et al.*, 2007; Stephens *et al.*, 2007; Boudreau *et al.*, 2008; Lucas *et al.*, 2008)	(Neeff *et al.*, 2005; Hyde *et al.*, 2007; Saatchi *et al.*, 2007; Le Toan *et al.*, 2008)

582

583 Table 3. RMSE of LiDAR and P-band radar for height and biomass

Figure legends

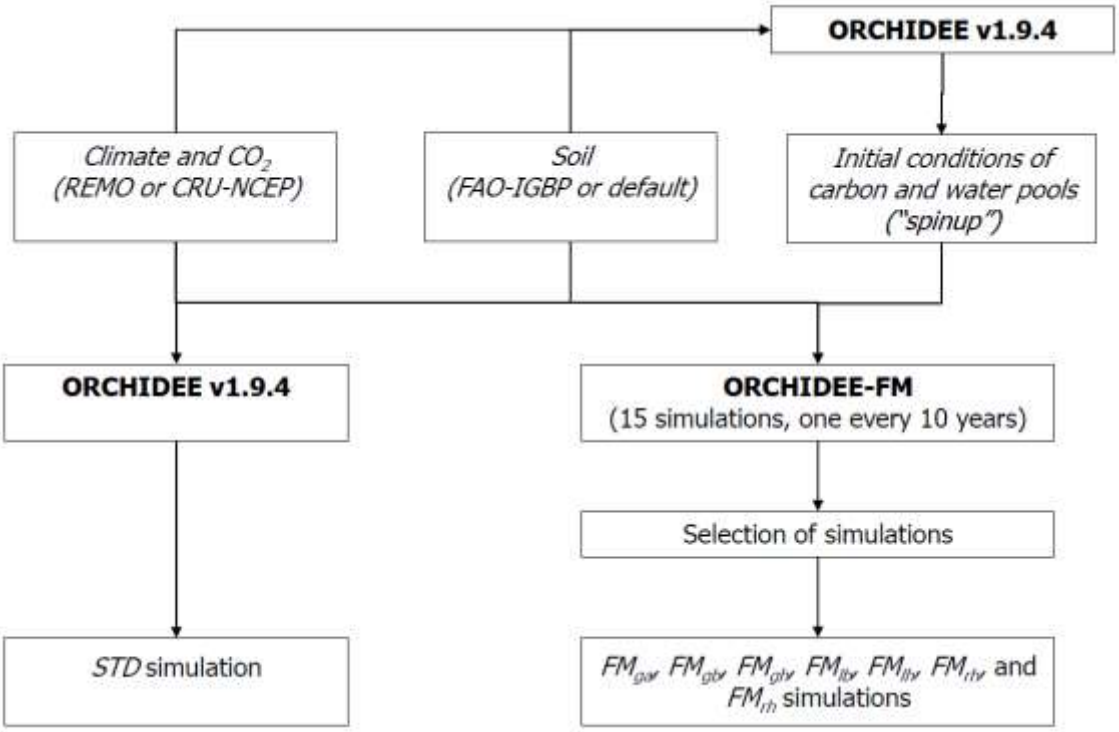

Figure 1. Combination of *input data (italic)* and **models (bold)** used in the simulation procedure

A typical "spinup" is used to generate intial conditions for both ORCHIDEE and ORCHIDEE-FM simulations. Out of the fifteen ORCHIDEE-FM simulations, seven are selected for each site according to their proximity to *in situ* or "pseudo remote sensing" measurements, and are given a specific name (FM_{ga}, FM_{gb}, …).

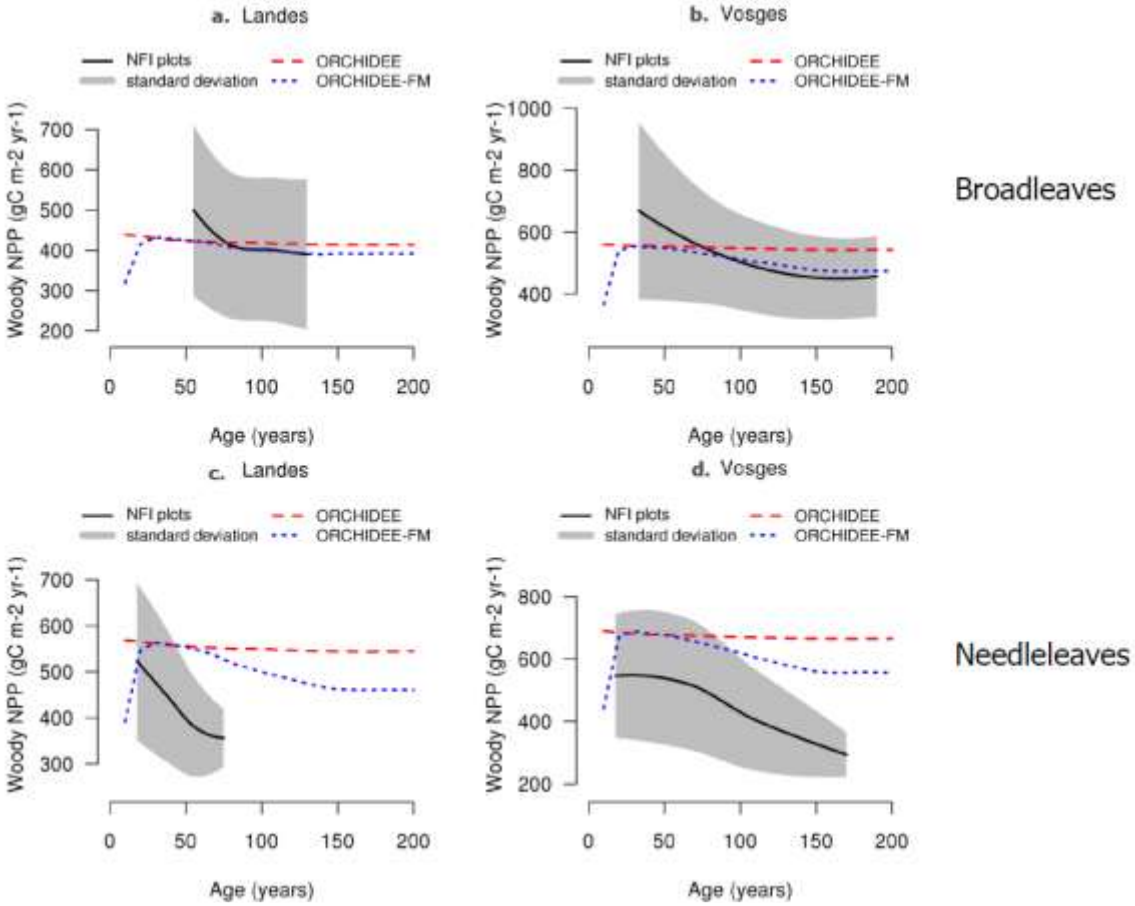

Figure 2. Age-related trend in woody NPP – IFN dataset

The black solid line and grey area respectively give the average and standard deviation of measured woody NPP in National Forest Inventory (NFI) broadleaf (a and b) or needleleaf (c and d) plots within a 50 km radius of the selected "Landes" (a and c) or "Vosges" (b and d) grid cell. Measurements are pooled per age class, and the resulting statistics per age class are smoothed using a "loess" algorithm (only age classes with 5 or more plots are retained). The large-dashed red curve and the small-dashed blue curve respectively give the wood increment in the *STD* and FM_{ga} simulations.

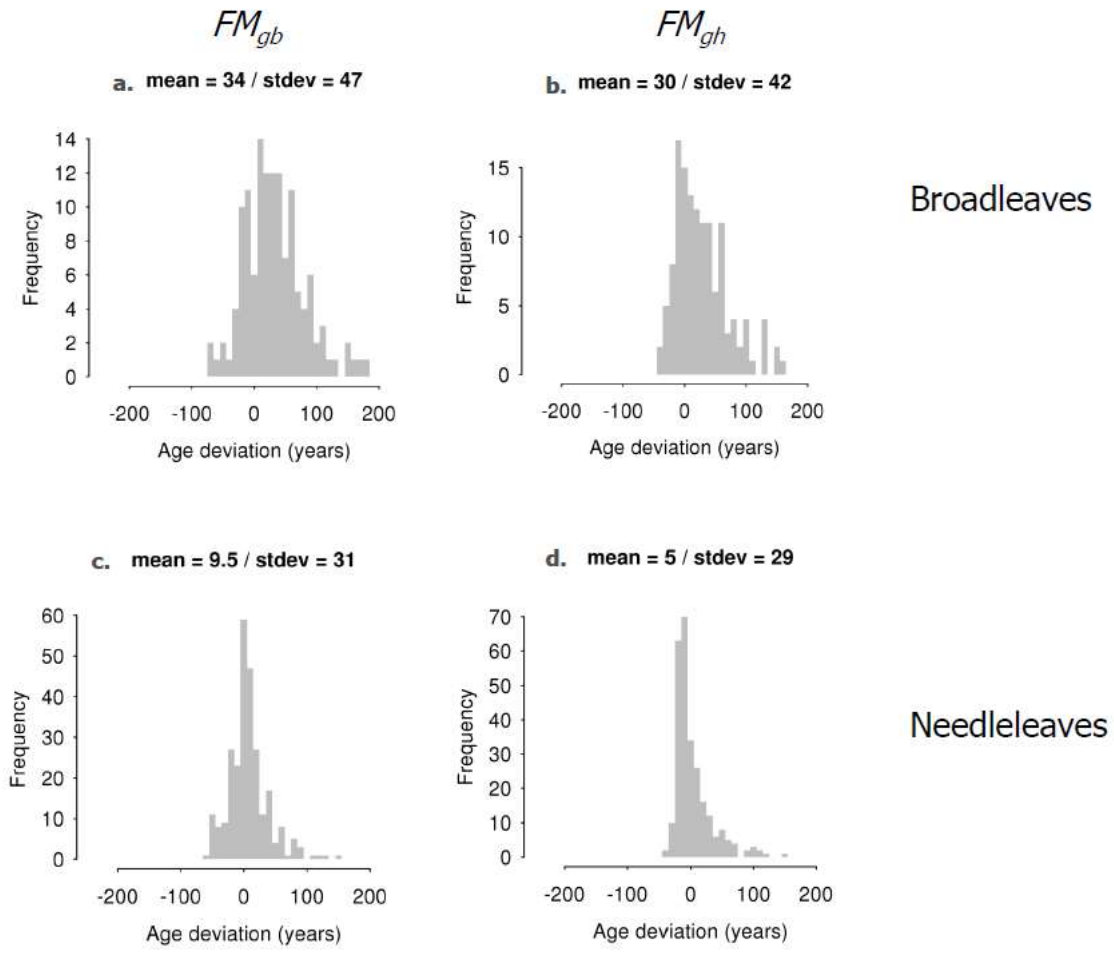

603

604 Figure 3. Age retrieval by assimilating biomass or height in ORCHIDEE-FM simulations –

605 IFN dataset

606 The difference between the age retrieved by biomass (FM_{gb} simulation, a and c) or

607 height (FM_{gh} simulation, b and d) assimilation in ORCHIDEE-FM and the *in situ* estimates

608 (IFN dataset) is presented as a frequency distribution for the 201 broadleaf plots (a and

609 b) and the 328 needleleaf plots (c and d) of the combined "Landes" and "Vosges"

610 locations. A negative value indicates that the simulated age is higher than the

611 measurement.

612

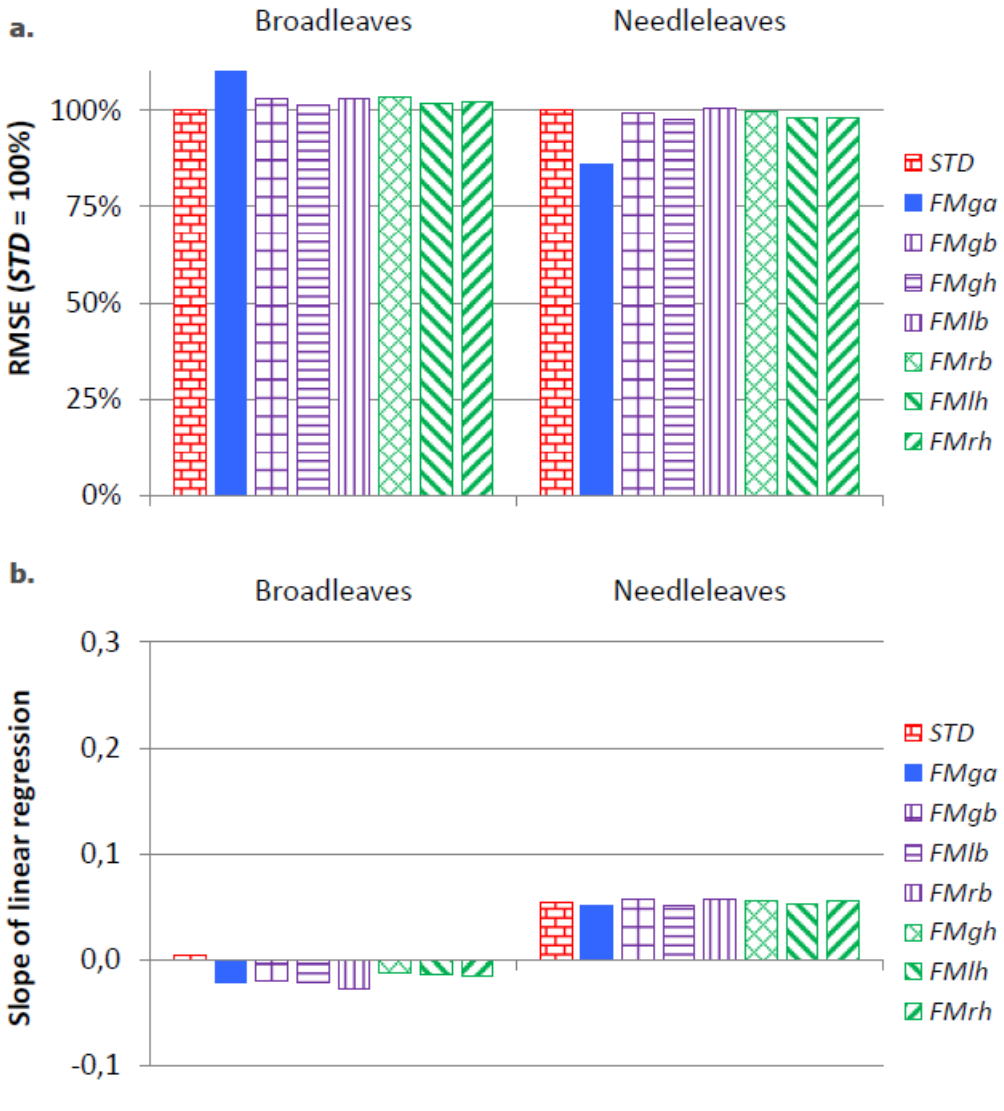

613

614 Figure 4. Improvement in simulated woody NPP – IFN dataset

615 The histograms compare two performance indexes for seven simulations: the RMSE (a)

616 and the slope of the linear regression between data and simulation (b). Four groups of

617 simulations are distinguished: *STD* (brick red) using the standard version of ORCHIDEE,

618 FM_{ga} (full blue) assimilating age in ORCHIDEE-FM, FM_{gb}, FM_{lb} and FM_{rb} (vertical and

horizontal dashed purple) assimilating biomass in ORCHIDEE-FM, and FM_{gh}, FM_{lh} and FM_{rh} (diagonal dashed green) assimilating height in ORCHIDEE-FM. For a full explanation of simulations names, see part 2.3.2, Appendix E and

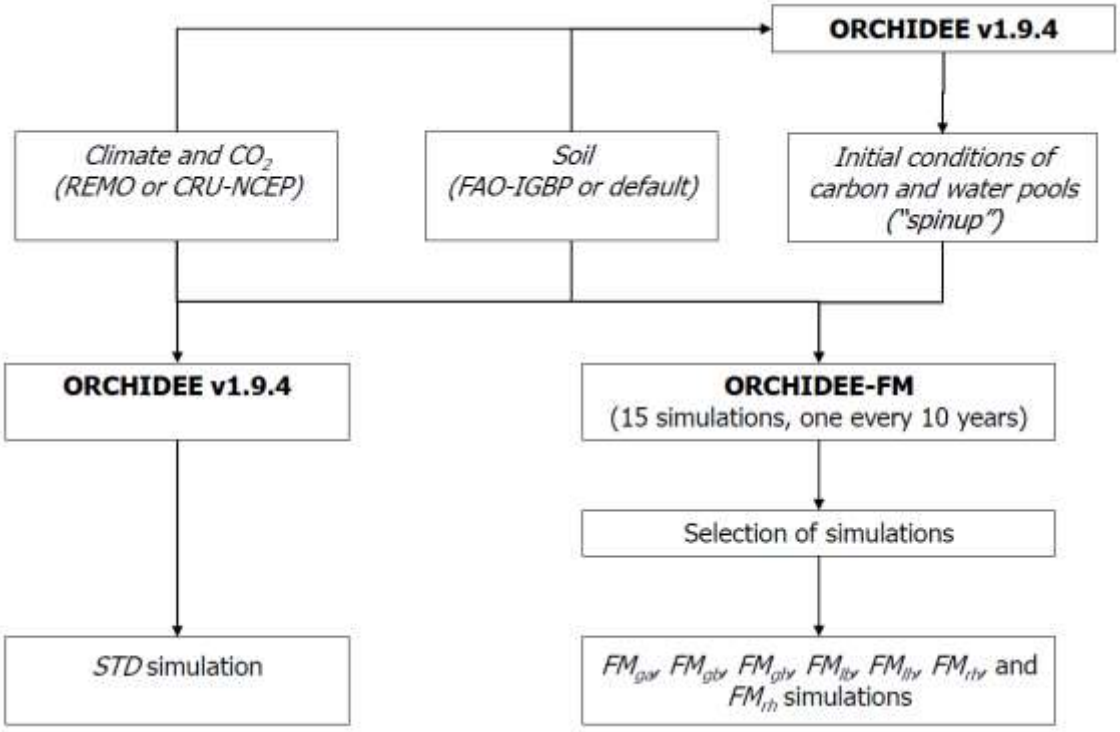

Figure 1.

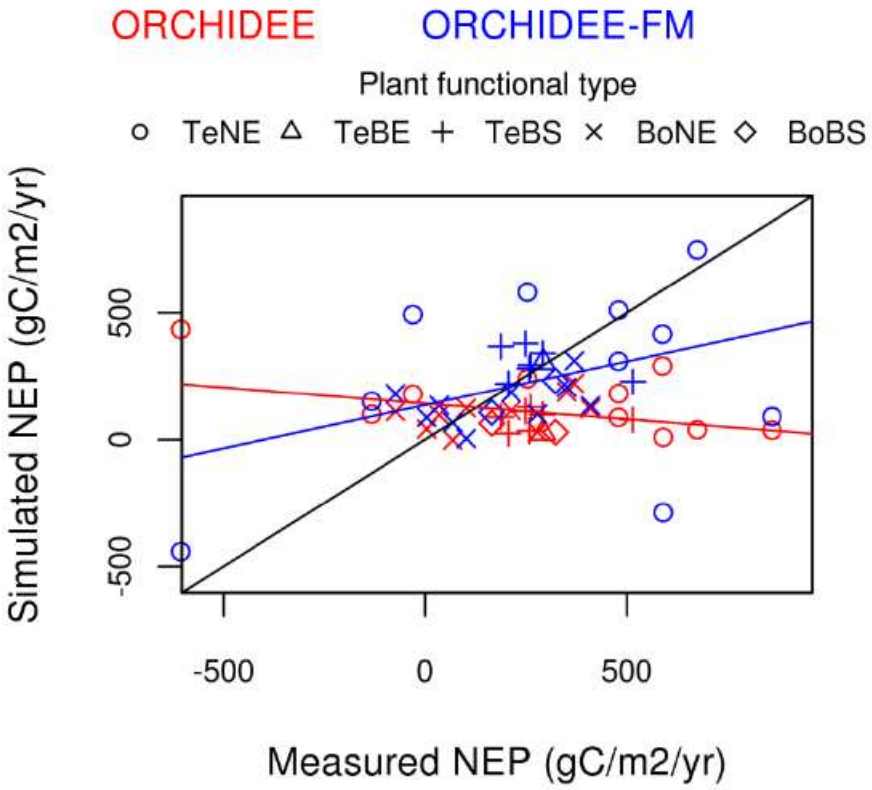

625

626 Figure 5. Simulation of NEP with age assimilation – global flux dataset

627 The values of the *STD* simulation are shown in red, while those of the FM_{ga} simulation

628 are shown in blue. The red and blue lines represent the respective linear trends of these

629 plot series. A different font is used for each plant functional type, with the following

630 code: TeNE for tempereate needleleaf evergreen, TeBE for temperate broadleaf

631 evergreen, TeBS for temperate broadleaf summergreen, BoNE for boreal needleleaf

632 evergreen, and BoBS for boreal broadleaf summergreen.

633

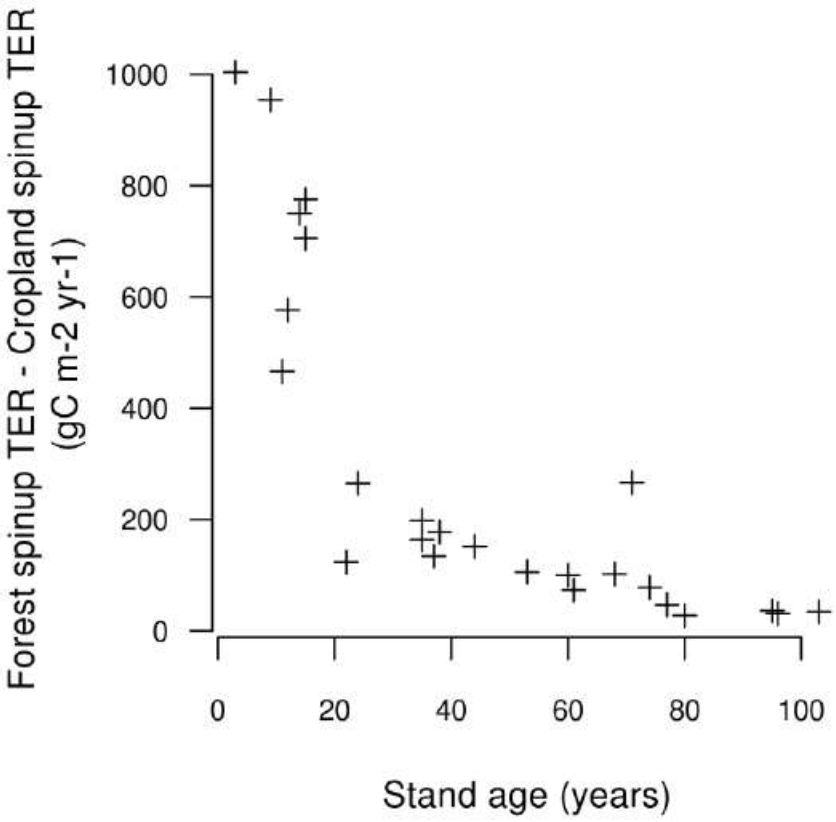

634

635 Figure 6. Difference in simulated TER between forest regrowth and reforestation

636 In the “Forest spinup” case, the intial conditions of the simulation correspond to the

637 clear-cut of a mature forest whereas in the “Cropland spinup” case, the initial conditions

638 of the simulation correspond to a cropland.

639

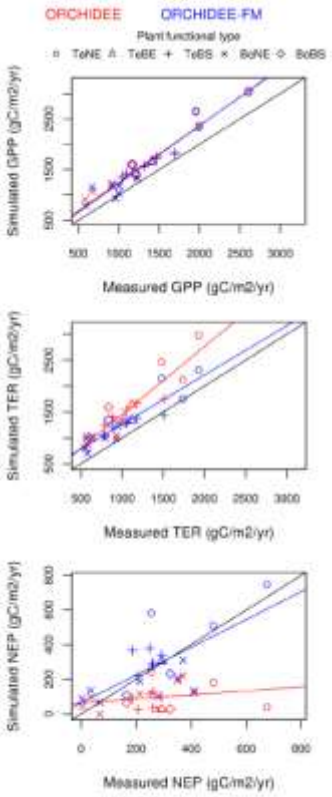

640

641 Figure 7. Simulation of GPP, TER and NEP with age assimilation – screened dataset

642 The values of the *STD* simulation are shown in red, while those of the FM_{ga} simulation

643 are shown in blue. The red and blue lines represent the respective linear trends of these

644 plot series. A different font is used for each plant functional type, with the following

645 code: TeNE for tempereate needleleaf evergreen, TeBE for temperate broadleaf

646 evergreen, TeBS for temperate broadleaf summergreen, BoNE for boreal needleleaf

647 evergreen, and BoBS for boreal broadleaf summergreen.

648

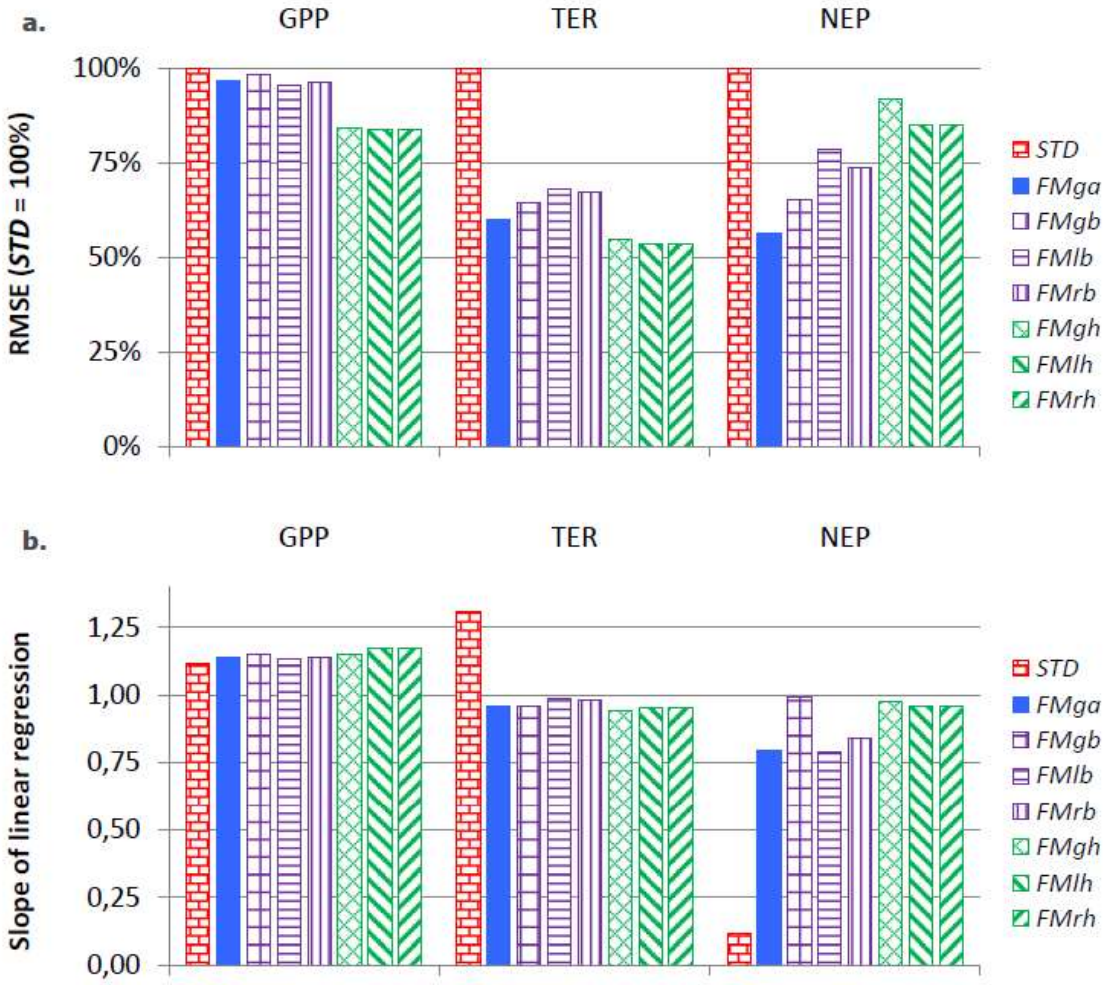

649

650 Figure 8. Improvement in simulated GPP, TER and NEP – screened dataset

651 The histograms compare two performance indexes for seven simulations: the RMSE (a)
652 and the slope of the linear regression between data and simulation (b). Four groups of
653 simulations are distinguished: *STD* (brick red) using the standard version of ORCHIDEE,
654 FM_{ga} (full blue) assimilating age in ORCHIDEE-FM, FM_{gb}, FM_{lb} and FM_{rb} (vertical and
655 horizontal dashed purple) assimilating biomass in ORCHIDEE-FM, and FM_{gh}, FM_{lh} and
656 FM_{rh} (diagonal dashed green) assimilating height in ORCHIDEE-FM. For a full explanation

657 of simulations names, see part 2.3.2, Appendix E and

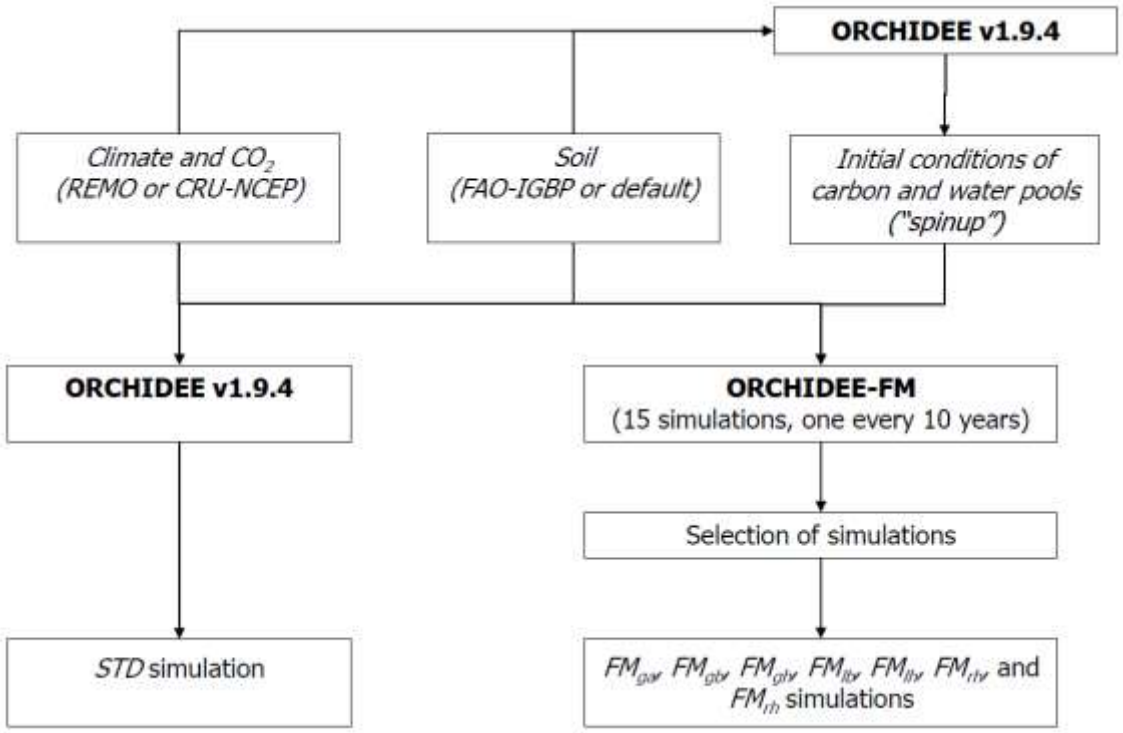

658

659 Figure 1.

660

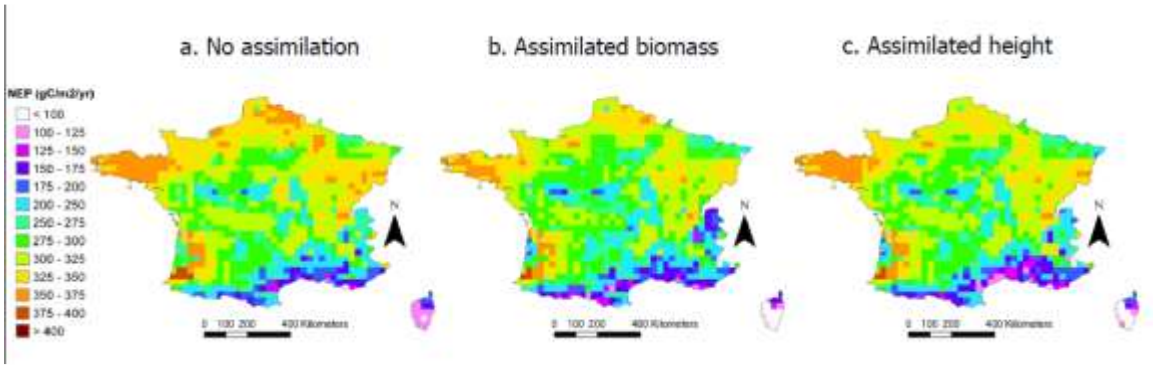

661

662 Figure 9. Maps of simulated NEP assimilated data-derived maps of height and volume

663 The average NEP in the 1990s is obtained from a single simulation of ORCHIDEE-FM for

664 the 40-50 age class (a), by selecting for each grid cell the ORCHIDEE-FM age-class with

665 closest biomass to the IFN-derived map (b), or by selecting for each grid cell the

666 ORCHIDEE-FM age-class with closest height to the IFN-derived map (c).

667

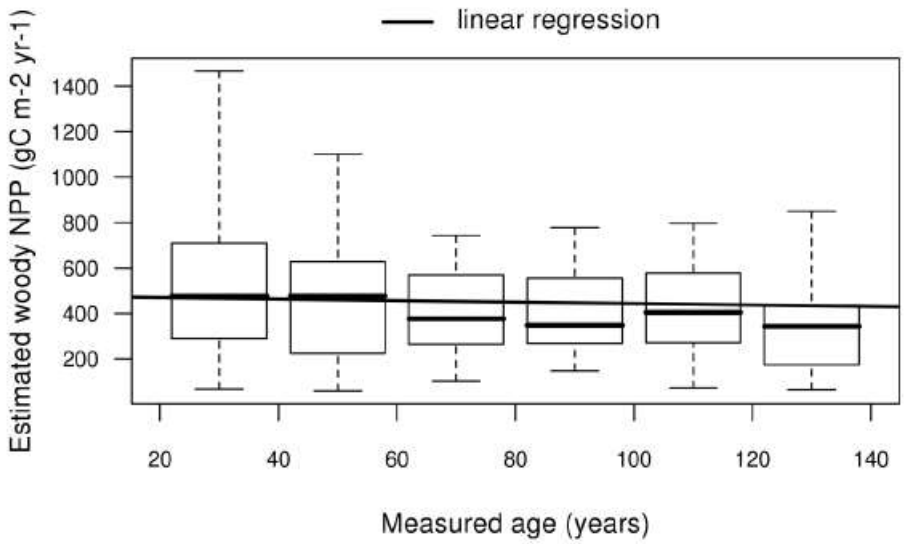

668

669 Figure 10. Evolution of woody NPP with age for broadleaves in the IFN dataset

670 For a given age class, the whisker plot represents successively the mean, 1st and 3rd

671 quartile, and extreme values within a distance of twice the interquartile from the box.

672

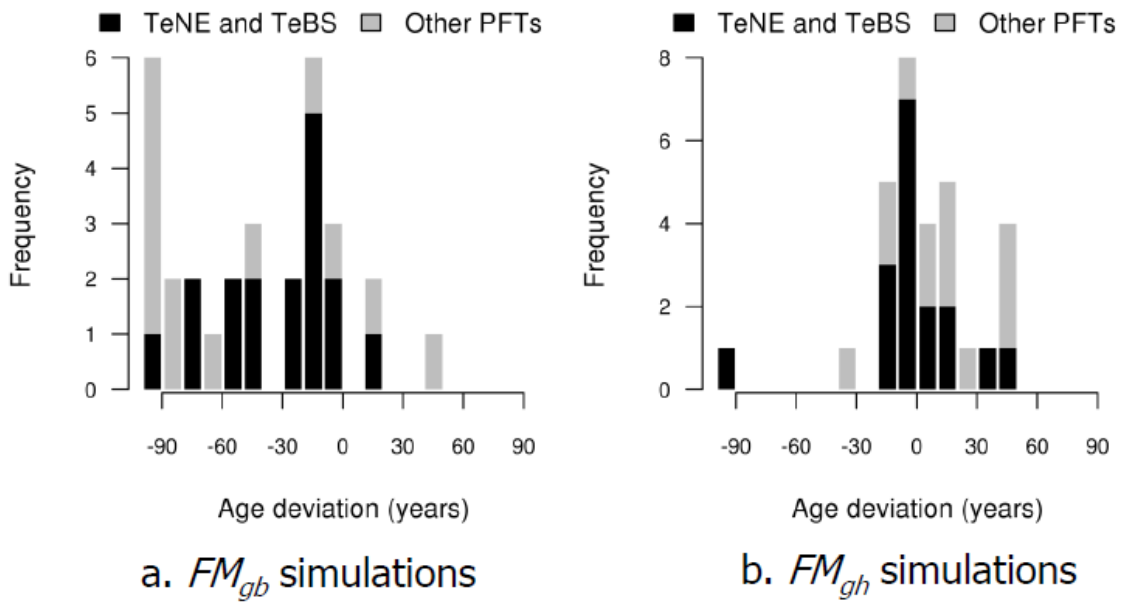

673

674 Figure 11. Age retrieval by assimilating biomass (a) or height (b) in ORCHIDEE-FM

675 simulations – global flux dataset

676 The difference between the age retrieved by biomass (FM_{gb} simulation, a) or height

677 (FM_{gh} simulation, b) assimilation in ORCHIDEE-FM and the in situ estimates (global flux

678 dataset) is presented as a frequency distribution for the 31 sites. A negative value

679 indicates that the simulated age is higher than the measurement.

680

681

682 Baldocchi, D., Falge, E., Gu, L.H., Olson, R., Hollinger, D., Running, S., Anthoni, P.,
683 Bernhofer, C., Davis, K., Evans, R., Fuentes, J., Goldstein, A., Katul, G., Law, B., Lee, X.H.,
684 Malhi, Y., Meyers, T., Munger, W., Oechel, W., U, K.T.P., Pilegaard, K., Schmid, H.P.,
685 Valentini, R., Verma, S., Vesala, T., Wilson, K., Wofsy, S., 2001. FLUXNET: A new tool to
686 study the temporal and spatial variability of ecosystem-scale carbon dioxide, water
687 vapor, and energy flux densities. Bulletin of the American Meteorological Society 82,
688 2415-2434.
689 Balzter, H., Luckman, A., Skinner, L., Rowland, C., Dawson, T., 2007a. Observations of
690 forest stand top height and mean height from interferometric SAR and LiDAR over a

691 conifer plantation at Thetford Forest, UK. International Journal of Remote Sensing 28,
692 1173-1197.
693 Balzter, H., Rowland, C.S., Saich, P., 2007b. Forest canopy height and carbon estimation
694 at Monks Wood National Nature Reserve, UK, using dual-wavelength SAR
695 interferometry. Remote Sensing of Environment 108, 224-239.
696 Bellassen, V., Le Maire, G., Dhote, J.F., Viovy, N., Ciais, P., 2010a. Modeling forest
697 management within a global vegetation model – Part 1: model structure and general
698 behaviour. Ecological Modelling 221, 2458–2474.
699 Bellassen, V., Le Maire, G., Guin, O., Dhote, J.F., Viovy, N., Ciais, P., 2010b. Modeling
700 forest management within a global vegetation model – Part 2: model validation from
701 tree to continental scale. Ecological Modelling in press.
702 Boudreau, J., Nelson, R.F., Margolis, H.A., Beaudoin, A., Guindon, L., Kimes, D.S., 2008.
703 Regional aboveground forest biomass using airborne and spaceborne LiDAR in Québec.
704 Remote Sensing of Environment 112, 3876.
705 Breidenbach, J., Koch, B., Kandler, G., Kleusberg, A., 2008. Quantifying the influence of
706 slope, aspect, crown shape and stem density on the estimation of tree height at plot
707 level using lidar and InSAR data. International Journal of Remote Sensing 29, 1511-1536.
708 Carvalhais, N., Reichstein, M., Ciais, P., Collatz, G.J., Mahecha, M., Montagnani, L.,
709 Papale, D., Rambal, S., Seixas, J., 2010. Identification of Vegetation and Soil Carbon Pools
710 out of Equilibrium in a Process Model via Eddy Covariance and Biometric Constraints.
711 Global Change Biology in press.
712 Deleuze, C., Pain, O., Dhote, J.F., Herve, J.C., 2004. A flexible radial increment model for
713 individual trees in pure even-aged stands. Annals of Forest Science 61, 327-335.
714 Demarty, J., Chevallier, F., Friend, A.D., Viovy, N., Piao, S., Ciais, P., 2007. Assimilation of
715 global MODIS leaf area index retrievals within a terrestrial biosphere model.
716 Geophysical Research Letters 34, 6.
717 Desai, A.R., Moorcroft, P.R., Bolstad, P.V., Davis, K.J., 2007. Regional carbon fluxes from
718 an observationally constrained dynamic ecosystem model: Impacts of disturbance, CO2
719 fertilization, and heterogeneous land cover. Journal of Geophysical Research-
720 Biogeosciences 112.
721 Dhôte, J.-F., Hervé, J.-C., 2000. Changements de productivité dans quatre forêts de
722 chênes sessiles depuis 1930 : une approche au niveau du peuplement. Ann. For. Sci. 57,
723 651-680.
724 Drake, J.B., Dubayah, R.O., Knox, R.G., Clark, D.B., Blair, J.B., 2002. Sensitivity of large-
725 footprint lidar to canopy structure and biomass in a neotropical rainforest. Remote
726 Sensing of Environment 81, 378-392.
727 Dubois-Fernandez, P.C., Souyris, J.C., Angelliaume, S., Garestier, F., 2008. The Compact
728 Polarimetry Alternative for Spaceborne SAR at Low Frequency. Ieee Transactions on
729 Geoscience and Remote Sensing 46, 3208-3222.
730 Dufrene, E., Davi, H., Francois, C., le Maire, G., Le Dantec, V., Granier, A., 2005.
731 Modelling carbon and water cycles in a beech forest Part I: Model description and
732 uncertainty analysis on modelled NEE. Ecological Modelling 185, 407-436.

733 Durrieu, S., 2010. Lidar for Earth and Forests. Proposal in response to the ESA Call for
734 Earth Explorer Opportunity Mission EE-8. CEMAGREF, Montpellier, France, 5 p.
735 Friedlingstein, P., Joel, G., Field, C.B., Fung, I.Y., 1999. Toward an allocation scheme for
736 global terrestrial carbon models. Global Change Biology 5, 755-770.
737 Grant, R.F., Black, T.A., Humphreys, E.R., Morgenstern, K., 2007. Changes in net
738 ecosystem productivity with forest age following clearcutting of a coastal Douglas-fir
739 forest: testing a mathematical model with eddy covariance measurements along a
740 forest chronosequence. Tree Physiology 27, 115-131.
741 Hajnsek, I., Kugler, F., Lee, S.K., Papathanassiou, K.P., 2009. Tropical-Forest-Parameter
742 Estimation by Means of Pol-InSAR: The INDREX-II Campaign. Ieee Transactions on
743 Geoscience and Remote Sensing 47, 481-493.
744 Hyde, P., Nelson, R., Kimes, D., Levine, E., 2007. Exploring LIDAR-RaDAR synergy -
745 predicting aboveground biomass in a southwestern ponderosa pine forest using LiDAR,
746 SAR and InSAR. Remote Sensing of Environment 106, 28-38.
747 IFN, 2006. Observer la forêt française : mission première de l'IFN. L'IF, 12.
748 IPCC, 2003. Good Practice Guidance for Land-Use, Land-Use Change and Forestry.
749 Intergovernmental Panel on Climate Change, Kanagawa, Japan, 534 p.
750 JRC, 2009. European Forest Yield Table's database,
751 http://afoludata.jrc.ec.europa.eu/DS_Free/abc_intro.cfm.
752 Kalnay, E., Kanamitsu, M., Kistler, R., Collins, W., Deaven, D., Gandin, L., Iredell, M.,
753 Saha, S., White, G., Woollen, J., Zhu, Y., Chelliah, M., Ebisuzaki, W., Higgins, W.,
754 Janowiak, J., Mo, K.C., Ropelewski, C., Wang, J., Leetmaa, A., Reynolds, R., Jenne, R.,
755 Joseph, D., 1996. The NCEP/NCAR 40-year reanalysis project. Bulletin of the American
756 Meteorological Society 77, 437-471.
757 Krinner, G., Viovy, N., de Noblet-Ducoudre, N., Ogee, J., Polcher, J., Friedlingstein, P.,
758 Ciais, P., Sitch, S., Prentice, I.C., 2005. A dynamic global vegetation model for studies of
759 the coupled atmosphere-biosphere system. Global Biogeochemical Cycles 19, 44.
760 Le Quere, C., Raupach, M.R., Canadell, J.G., Marland, G., Bopp, L., Ciais, P., Conway, T.J.,
761 Doney, S.C., Feely, R.A., Foster, P., Friedlingstein, P., Gurney, K., Houghton, R.A., House,
762 J.I., Huntingford, C., Levy, P.E., Lomas, M.R., Majkut, J., Metzl, N., Ometto, J.P., Peters,
763 G.P., Prentice, I.C., Randerson, J.T., Running, S.W., Sarmiento, J.L., Schuster, U., Sitch, S.,
764 Takahashi, T., Viovy, N., van der Werf, G.R., Woodward, F.I., 2009. Trends in the sources
765 and sinks of carbon dioxide. Nature Geoscience 2, 831-836.
766 Le Toan, T., Baltzer, H., Paillou, P., Papathanassiou, K., Plummer, S., Quegan, S., Rocca,
767 F., Ulander, L., 2008. Candidate Earth Explorer Core Mission - Biomass. ESA, Noordwijk,
768 124 p.
769 Lefsky, M.A., Harding, D.J., Keller, M., Cohen, W.B., Carabajal, C.C., Espirito-Santo, F.D.,
770 Hunter, M.O., de Oliveira, R., 2005a. Estimates of forest canopy height and aboveground
771 biomass using ICESat. Geophysical Research Letters 32.
772 Lefsky, M.A., Turner, D.P., Guzy, M., Cohen, W.B., 2005b. Combining lidar estimates of
773 aboveground biomass and Landsat estimates of stand age for spatially extensive
774 validation of modeled forest productivity. Remote Sensing of Environment 95, 549.

Lim, K.S., Treitz, P.M., 2004. Estimation of above ground forest biomass from airborne discrete return laser scanner data using canopy-based quantile estimators. In, pp. 558-570.
Lindner, M., Lucht, W., Bouriaud, O., Green, T., Janssens, I., 2004. Specific Study on Forest Greenhouse Gas Budget. CarboEurope-GHG, Jena, 62 p.
Loustau, D., Bosc, A., Colin, A., Ogee, J., Davi, H., Francois, C., Dufrene, E., Deque, M., Cloppet, E., Arrouays, D., Le Bas, C., Saby, N., Pignard, G., Hamza, N., Granier, A., Breda, N., Ciais, P., Viovy, N., Delage, F., 2005. Modeling climate change effects on the potential production of French plains forests at the sub-regional level. Tree Physiology 25, 813-823.
Lucas, R.M., Lee, A.C., Bunting, P.J., 2008. Retrieving forest biomass through integration of CASI and LiDAR data. In, pp. 1553-1577.
Luyssaert, S., Ciais, P., Piao, S.L., Schulze, E.D., Jung, M., Zaehle, S., Schelhaas, M.J., Reichstein, M., Churkina, G., Papale, D., Abril, G., Beer, C., Grace, J., Loustau, D., Matteucci, G., Magnani, F., Nabuurs, G.J., Verbeeck, H., Sulkava, M., van der Werf, G.R., Janssens, I.A., Team, C.-I.S., 2010. The European carbon balance. Part 3: forests. Global Change Biology 16, 1429-1450.
Luyssaert, S., Inglima, I., Jung, M., Richardson, A.D., Reichsteins, M., Papale, D., Piao, S.L., Schulzes, E.D., Wingate, L., Matteucci, G., Aragao, L., Aubinet, M., Beers, C., Bernhoffer, C., Black, K.G., Bonal, D., Bonnefond, J.M., Chambers, J., Ciais, P., Cook, B., Davis, K.J., Dolman, A.J., Gielen, B., Goulden, M., Grace, J., Granier, A., Grelle, A., Griffis, T., Grunwald, T., Guidolotti, G., Hanson, P.J., Harding, R., Hollinger, D.Y., Hutyra, L.R., Kolar, P., Kruijt, B., Kutsch, W., Lagergren, F., Laurila, T., Law, B.E., Le Maire, G., Lindroth, A., Loustau, D., Malhi, Y., Mateus, J., Migliavacca, M., Misson, L., Montagnani, L., Moncrieff, J., Moors, E., Munger, J.W., Nikinmaa, E., Ollinger, S.V., Pita, G., Rebmann, C., Roupsard, O., Saigusa, N., Sanz, M.J., Seufert, G., Sierra, C., Smith, M.L., Tang, J., Valentini, R., Vesala, T., Janssens, I.A., 2007. CO2 balance of boreal, temperate, and tropical forests derived from a global database. Global Change Biology 13, 2509-2537.
Luyssaert, S., Reichstein, M., Schulze, E.D., Janssens, I.A., Law, B.E., Papale, D., Dragoni, D., Goulden, M.L., Granier, A., Kutsch, W.L., Linder, S., Matteucci, G., Moors, E., Munger, J.W., Pilegaard, K., Saunders, M., Falge, E.M., 2009. Toward a consistency cross-check of eddy covariance flux-based and biometric estimates of ecosystem carbon balance. Global Biogeochemical Cycles 23.
Magnani, F., Mencuccini, M., Borghetti, M., Berbigier, P., Berninger, F., Delzon, S., Grelle, A., Hari, P., Jarvis, P.G., Kolari, P., Kowalski, A.S., Lankreijer, H., Law, B.E., Lindroth, A., Loustau, D., Manca, G., Moncrieff, J.B., Rayment, M., Tedeschi, V., Valentini, R., Grace, J., 2007. The human footprint in the carbon cycle of temperate and boreal forests. Nature 447, 848-850.
Masera, O.R., Garza-Caligaris, J.F., Kanninen, M., Karjalainen, T., Liski, J., Nabuurs, G.J., Pussinen, A., de Jong, B.H.J., Mohren, G.M.J., Tz, 2003. Modeling carbon sequestration in afforestation, agroforestry and forest management projects: the CO2FIX V.2 approach. Ecological Modelling 164, 177-199.

817 Means, J.E., Acker, S.A., Harding, D.J., Blair, J.B., Lefsky, M.A., Cohen, W.B., Harmon,
818 M.E., McKee, W.A., 1999. Use of large-footprint scanning airborne lidar to estimate
819 forest stand characteristics in the Western Cascades of Oregon. Remote Sensing of
820 Environment 67, 298-308.
821 Mitchell, S., Beven, K., Freer, J., 2009. Multiple sources of predictive uncertainty in
822 modeled estimates of net ecosystem CO2 exchange. Ecological Modelling 220, 3259-
823 3270.
824 Mitchell, T.D., Jones, P.D., 2005. An improved method of constructing a database of
825 monthly climate observations and associated high-resolution grids. International Journal
826 of Climatology 25, 693-712.
827 Moorcroft, P.R., Hurtt, G.C., Pacala, S.W., 2001. A method for scaling vegetation
828 dynamics: The ecosystem demography model (ED). Ecological Monographs 71, 557-585.
829 Nabuurs, G.J., Hengeveld, G., Heidema, N., Brus, D., Goedhart, P., Walvoort, D., van den
830 Wyngaert, I., van der Werf, B., Tröltzsch, K., Lindner, M., Zanchi, G., Gallaun, H.,
831 Schwaiger, H., Teobaldelli, M., Seufert, G., Kenter, B., 2008. Mapping the continent: High
832 resolution forest resource analyses of European forests. The European Carbon Balance -
833 Research Highlights 2008. CarboEurope-IP (eds.), 4 p.
834 Naesset, E., 2009. Effects of different sensors, flying altitudes, and pulse repetition
835 frequencies on forest canopy metrics and biophysical stand properties derived from
836 small-footprint airborne laser data. Remote Sensing of Environment 113, 148-159.
837 Neeff, T., Dutra, L.V., dos Santos, J.R., Freitas, C.D., Araujo, L.S., 2005. Tropical forest
838 measurement by interferometric height modeling and P-band radar backscatter. Forest
839 Science 51, 585-594.
840 Nelson, R.F., Parker, G.G., Hom, M., 2003. A portable airborne laser system for forest
841 inventory. American Society for Photogrammetry and Remote Sensing, Bethesda, USA, 7
842 p.
843 Nunery, J.S., Keeton, W.S., 2010. Forest carbon storage in the northeastern United
844 States: Net effects of harvesting frequency, post-harvest retention, and wood products.
845 Forest Ecology and Management 259, 1363-1375.
846 Pan, Y., Chen, J.M., Birdsey, R., McCullough, K., He, L., Deng, F., 2010. Age structure and
847 disturbance legacy of North American forests. Biogeosciences Discuss. 7, 979-1020.
848 Piao, S.L., Fang, J.Y., Ciais, P., Peylin, P., Huang, Y., Sitch, S., Wang, T., 2009. The carbon
849 balance of terrestrial ecosystems in China. Nature 458, 1009-U1082.
850 Porté, A., 1999. Modélisation des effets du bilan hydrique sur la production primaire et
851 la croissance d'un couvert de pin maritime (Pinus pinaster Ait.) en lande humide,
852 University of Paris XI, Orsay, France, 140 p.
853 Pretzsch, H., Biber, P., Durský, J., 2002. The single tree-based stand simulator SILVA:
854 construction, application and evaluation. Forest Ecology and Management 162, 3.
855 Reineke, L.H., 1933. Perfecting a stand-density index for even-aged forests. Journal of
856 Agricultural Research 46, 627-638.
857 Rubinstein, R.Y., Kroese, D.P., 1981. Simulation and the Monte Carlo Method. Wiley,
858 New York, USAp.

859 Saatchi, S., Halligan, K., Despain, D.G., Crabtree, R.L., 2007. Estimation of forest fuel load
860 from radar remote sensing. Ieee Transactions on Geoscience and Remote Sensing 45,
861 1726-1740.
862 Santaren, D., 2006. Optimisation des paramètres du modèle de biosphère ORCHIDEE à
863 partir de mesures sur site des flux de carbone, d'eau et d'énergie, Université Versailles
864 Saint-Quentin, Versailles, 190 p.
865 Sarrat, C., Noilhan, J., Lacarrere, P., Ceschia, E., Ciais, P., Dolman, A.J., Elbers, J.A.,
866 Gerbig, C., Gioli, B., Lauvaux, T., Miglietta, F., Neininger, B., Ramonet, M., Vellinga, O.,
867 Bonnefond, J.M., 2009. Mesoscale modelling of the CO2 interactions between the
868 surface and the atmosphere applied to the April 2007 CERES field experiment.
869 Biogeosciences 6, 633-646.
870 Sato, H., Itoh, A., Kohyama, T., 2007. SEIB-DGVM: A new dynamic global vegetation
871 model using a spatially explicit individual-based approach. Ecological Modelling 200,
872 279-307.
873 Sitch, S., Smith, B., Prentice, I.C., Arneth, A., Bondeau, A., Cramer, W., Kaplan, J.O., Levis,
874 S., Lucht, W., Sykes, M.T., Thonicke, K., Venevsky, S., 2003. Evaluation of ecosystem
875 dynamics, plant geography and terrestrial carbon cycling in the LPJ dynamic global
876 vegetation model. Global Change Biology 9, 161-185.
877 Stephens, P.R., Watt, P.J., Loubser, D., Haywood, A., Kimberley, M.O., 2007. Estimation
878 of carbon stocks in New Zealand planted forests using airborne scanning LiDAR. IAPRS
879 36, 389-394.
880 Thornton, P.E., Law, B.E., Gholz, H.L., Clark, K.L., Falge, E., Ellsworth, D.S., Golstein, A.H.,
881 Monson, R.K., Hollinger, D., Falk, M., Chen, J., Sparks, J.P., 2002. Modeling and
882 measuring the effects of disturbance history and climate on carbon and water budgets
883 in evergreen needleleaf forests. Agricultural and Forest Meteorology 113, 185-222.
884 Vannière, B., 1984. Tables de production pour les forêts françaises. Ecole Nationale du
885 Génie Rural, des Eaux et des Forêts, Nancy, 160 p.
886 Vetter, M., Churkina, G., Jung, M., Reichstein, M., Zaehle, S., Bondeau, A., Chen, Y., Ciais,
887 P., Feser, F., Freibauer, A., Geyer, R., Jones, C., Papale, D., Tenhunen, J., Tomelleri, E.,
888 Trusilova, K., Viovy, N., Heimann, M., 2008. Analyzing the causes and spatial pattern of
889 the European 2003 carbon flux anomaly using seven models. Biogeosciences 5, 561-583.
890 Watt, P.J., Haywood, A., 2006. Evaluation of airborne scanning LiDAR generated data as
891 input into biomass/carbon models. No. 38A08068, Ministry for the Environment,
892 Wellington, New Zealand, 34 p.
893 Willmott, C.J., 1982. Some Comments on the Evaluation of Model Performance. Bulletin
894 of the American Meteorological Society 63, 1309-1313.
895 Zaehle, S., Friend, A.D., 2010. Carbon and nitrogen cycle dynamics in the O-CN land
896 surface model: 1. Model description, site-scale evaluation, and sensitivity to parameter
897 estimates. Global Biogeochemical Cycles 24.
898 Zaehle, S., Friend, A.D., Friedlingstein, P., Dentener, F., Peylin, P., Schulz, M., 2010.
899 Carbon and nitrogen cycle dynamics in the O-CN land surface model: 2. Role of the

900 nitrogen cycle in the historical terrestrial carbon balance. Global Biogeochemical Cycles
901 24.
902 Zaehle, S., Sitch, S., Prentice, I.C., Liski, J., Cramer, W., Erhard, M., Hickler, T., Smith, B.,
903 2006. The importance of age-related decline in forest NPP for modeling regional carbon
904 balances. Ecological Applications 16, 1555-1574.
905
906